CHAPTER ONE

Hyaluronan and Hyaluronan Fragments

Mary K. Cowman
Tandon School of Engineering, New York University, New York, NY, United States

Contents

ABBREVIATIONS

AFM	atomic force microscopy
ELISA	enzyme-linked immunosorbent assay
FRAP	fluorescence recovery after photobleaching
GAG	glycosaminoglycan
GPI	glycosylphosphatidylinositol
HA	hyaluronan
HABP	HA-binding protein (the G1-IGD-G2 portion of aggrecan)
IEX	ion-exchange chromatography
M	molecular mass

Advances in Carbohydrate Chemistry and Biochemistry, Volume 74
ISSN 0065-2318
https://doi.org/10.1016/bs.accb.2017.10.001

MALLS	multiangle laser light scattering
NMR	nuclear magnetic resonance
OA	osteoarthritis
PAGE	polyacrylamide gel electrophoresis
PMN	polymorphonuclear leukocytes
RA	rheumatoid arthritis
RNS	reactive nitrogen species
ROS	reactive oxygen species
SEC	size-exclusion chromatography
TAE	Tris–acetate–EDTA buffer
TBE	Tris–borate–EDTA buffer
UVB	ultraviolet light with wavelength of 280–315 nm

1. INTRODUCTION

Hyaluronan (hyaluronic acid, HA) is an extracellular polysaccharide of the glycosaminoglycan family. It has a simple repeating disaccharide sequence,[1] poly[(1→4)-β-D-glucopyranosyluronic acid-(1→3)-2-acetamido-2-deoxy-β-D-glucopyranosyl], with no evidence of heterogeneity or branching[2] (Fig. 1). The pK_a of the carboxylate group is about 3.2, making HA a polyanion with a charge spacing of nearly 1 nm at physiological pH. HA is the only glycosaminoglycan that is not covalently attached to a protein core. It is synthesized by hyaluronan synthase enzymes embedded in the plasma membrane, and it is extruded directly to the extracellular space.[3–5] In normal healthy tissues, HA is polydisperse in size,[6] with an average molecular mass (M) of about 6000 kDa, corresponding to a chain length of about 15,000 nm. The cross-sectional diameter of a chain is only about 0.5 nm, but the molecule adopts a rapidly changing expanded random coil conformation with a large effective hydrodynamic diameter in physiological saline solutions.[7] There is growing evidence for the existence of low-molecular-mass HA fragments in biological fluids and tissues, under inflammatory or other pathological conditions, and during development and remodeling processes.[8–10]

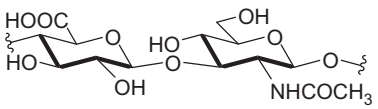

Fig. 1 Hyaluronan (HA) structure is a repeating disaccharide unit of poly[(1→4)-β-D-glucopyranosyluronic acid-(1→3)-2-acetamido-2-deoxy-β-D-glucopyranosyl].

HA is found widely distributed in vertebrate tissues and fluids, and it also occurs as a protective disguise in some bacteria.[11] In synovial fluid of articular joints, HA is present at sufficiently high concentration to provide a viscoelastic cushion to protect adjacent tissues, and it also acts as a lubricant between cartilage surfaces.[12–15] In the vitreous humor of the eye, HA supports and maintains a network of collagen fibers, protecting ocular tissues and maintaining a clear visual path between the lens and retina.[16] In solid tissues, the content of HA varies widely.[6] Tissues such as cartilage and skin have extensive extracellular matrices in which HA serves to bind and organize proteoglycans, providing a highly hydrated network to resist tissue compression.[17] Near the surface of cells, the pericellular matrix contains HA noncovalently tethered to cell-surface receptor proteins, where it serves to bind proteoglycans and maintain the osmotic and biomechanical properties of the cellular microenvironment.[18] HA affects the partition, transport, and binding interactions of proteins near the cell surface.[19,20] Through its interaction with receptor proteins, HA contributes to homeostatic control of cellular signaling pathways of importance in proliferation, migration, differentiation, tissue repair, tumor development and metastasis, and response to inflammation.[11,21] The simple covalent and conformational structure of HA, previously considered to serve only a protective mechanical function, is now associated with an extraordinary number of physiological functions. This versatility depends on differential cell signaling as a function of HA size and protein interactions.[9,22–24]

Purified HA provides a noninflammatory and nonimmunogenic biomaterial.[25–27] The current medical applications of HA are primarily based on its physicochemical properties. Solutions of unmodified HA exhibit high viscosity and elasticity, while shear thinning allows facile delivery through a narrow syringe needle. HA is used in ophthalmic surgery to cushion and protect the cornea during cataract extraction and intraocular lens replacement. Solutions of HA, in the presence or absence of additional chemically cross-linked HA, are delivered by intraarticular injection to relieve pain in patients with osteoarthritis. HA or its chemically cross-linked or derivatized forms are used for tissue augmentation, hydration, separation, and repair. Recent evidence for the cell-signaling properties of HA, including the observation that the beneficial properties of HA can continue long after the injected material has been eliminated from a tissue, suggests that new medical applications will be developed to leverage HA signaling and to direct desired changes in cell behavior and tissue properties.[10]

This chapter will describe experimental evidence concerning the structure and biological content of HA and its differences in healthy vs pathological conditions, with the goal of highlighting potential new diagnostic and therapeutic applications.

2. HA IN THE SOLID STATE AND AT SURFACES

X-ray diffraction studies of stretched fibers of HA reveal extended helices containing two, three, or four disaccharides per helical repeat.[28–31] The structures of the fully protonated acid form and the sodium and calcium salts of HA are single helices, but a double helical form was observed for a partially protonated potassium salt, and for the rubidium or ammonium salts of HA.[32,33] For NaHA, the rise per disaccharide residue in a threefold helix is ca. 0.85–0.95 nm, close to the fully extended length of ca. 1 nm. All other forms are similarly extended (0.82–0.98 nm per disaccharide), reflecting the inherently limited conformational freedom and the presence of stabilizing hydrogen bonds at the glycosidic linkages.

HA deposited on surfaces and imaged under vacuum by electron microscopy[34–37] or in air by using the tapping mode of atomic force microscopy (AFM)[38–46] shows a marked tendency for self-association unless bound proteins block HA–HA contact (Fig. 2). In part, this reflects poor adhesion of HA to the atomically flat surfaces used in AFM, such as weakly anionic mica or hydrophobic graphite. If deposited on mica in the presence of low

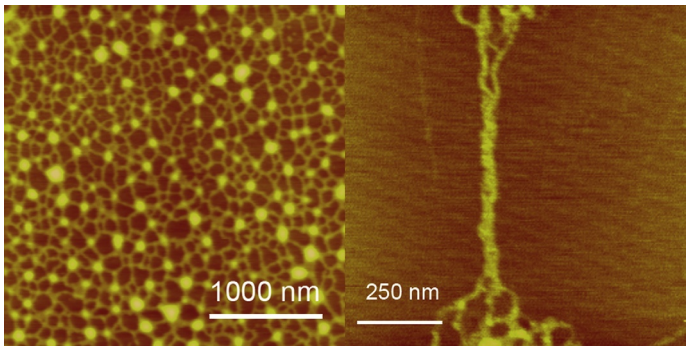

Fig. 2 AFM images of HA showing chain aggregation and formation of twisted fibrils when dried on a mica surface. *This figure has been adapted with permission from Cowman, M. K.; Spagnoli, C.; Kudasheva, D.; Li, M.; Dyal, A.; Kanai, S.; Balazs, E. A. Extended, Relaxed, and Condensed Conformations of Hyaluronan Observed by Atomic Force Microscopy.* Biophys. J. ***2005,*** 88, *590–602. Copyright 2005, The Biophysical Society.*

concentrations of NaCl or $MgCl_2$, and trapped in a thin layer of partially structured water at the surface, single chains of HA can adopt loosely helical coiled structures (Fig. 3A–C) that provide useful models for understanding HA conformation in solution. Partially condensed (pearl necklace) forms with almost uniformly spaced condensed balls are also commonly found due to weak surface attraction (Fig. 3D), but also because these are entropically favored structures for any crowded or poorly solvated polymer.[7]

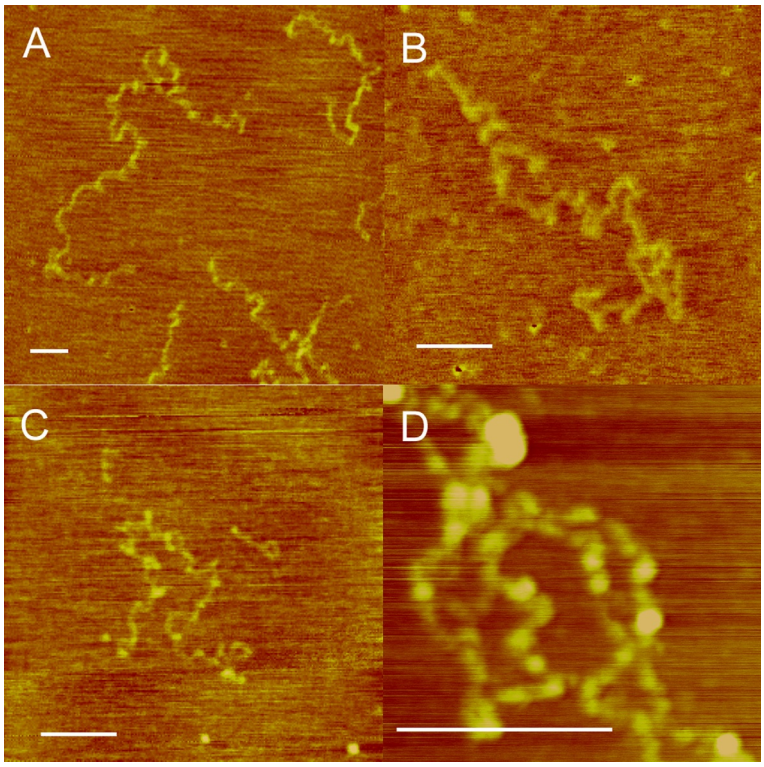

Fig. 3 AFM images of HA trapped in a thin layer of water on a mica surface showing relaxed coil and partially condensed forms. Bar equals 200 nm. *Images A, B, and D are reproduced with permission from Cowman, M. K.; Spagnoli, C.; Kudasheva, D.; Li, M.; Dyal, A.; Kanai, S.; Balazs, E. A. Extended, Relaxed, and Condensed Conformations of Hyaluronan Observed by Atomic Force Microscopy.* Biophys. J. ***2005,*** 88*, 590–602. Copyright 2005, The Biophysical Society. Image C is reproduced with permission from Cowman, M. K.; Spagnoli, C.; Kudasheva, D. S.; Matsuoka, S.; Balazs, E. A. Influence of Environment on Hyaluronan Shape. In* Hyaluronan: Structure, Metabolism, Biological Activities, Therapeutic Applications*; Balazs, E. A., Hascall, V. C., Eds. Matrix Biology Institute: Edgewater, NJ, 2005; Vol. 1, pp. 79–87. Copyright 2005, Matrix Biology Institute.*

3. HA IN DILUTE AND IN CROWDED SOLUTIONS

The medically important physicochemical properties of HA solutions are dependent on chain stiffness and length and the relatively low concentration above which nonideality effects due to mutual crowding of the macromolecules can be observed. These properties will be addressed first in terms of isolated chains in dilute solution, and then in terms of the effects of mutual macromolecular crowding observed in semidilute solutions.

In dilute solution HA chains are sufficiently separated that there is very little perturbation of the chain dimensions or dynamics due to neighbor interactions. Light-scattering data[47–50] indicate that high-molecular-mass HA adopts a worm-like chain in aqueous solution, with a radius of gyration that increases as the molecular mass to approximately the 0.6 power ($M^{0.6}$). Nuclear magnetic resonance studies[51–54] show that intramolecular hydrogen bonds spanning the glycosidic linkages are weak and dynamically formed and broken. ^{13}C NMR relaxation studies show that segmental motions of the polymer chain occur on the nanosecond timescale.

Measurement of the reduced viscosity (equal to the specific viscosity divided by the concentration, η_{sp}/c) as a function of concentration, and extrapolation to zero concentration, allows determination of the intrinsic viscosity ($[\eta]$), which is a measure of the specific volume, V_s, in cm^3/g, occupied by HA chains. For short HA chains with molecular mass less than about 37.5 kDa, the intrinsic viscosity depends on HA molecular mass to approximately the 1.2 power ($M^{1.2}$), whereas for longer chains intrinsic viscosity depends on $M^{0.80}$ (Fig. 4).[47,48,55–61] This reflects a change in the chain hydrodynamic properties from nearly rod-like to weakly coiled, effectively spherical, forms. Alternative methods for analyzing the experimental data for intrinsic viscosity show that it can be quantitatively matched by the worm-like coil model,[62–64] where the chain stiffness is characterized by a persistence length of about 4.5 nm. Chains shorter than about 20 persistence lengths behave rod-like, but longer chains can be modeled hydrodynamically as spheres. Using the measured intrinsic viscosity and the nonfree-draining ball model for HA, the effective hydrodynamic diameter for HA chains of different molecular mass can be calculated as shown in Table 1. This reveals an important aspect of HA structure in dilute aqueous salt solution. The diameter of an isolated HA chain grows rapidly with molecular mass such that the physiologically relevant 6000 kDa HA occupies a spherical domain (time- and ensemble-averaged) with a diameter of about

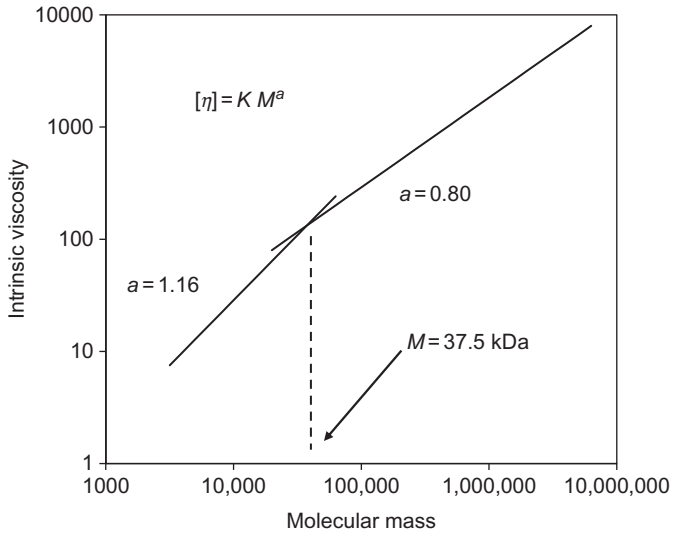

Fig. 4 Experimental dependence of intrinsic viscosity on molecular mass for HA in 0.15 M NaCl solution. Low-molecular-mass HA behaves like a rod-like, free-draining chain. Longer HA chains act like nonfree-draining sphere-like coils. *This figure has been adapted with permission from Cowman, M. K.; Matsuoka, S. The Intrinsic Viscosity of Hyaluronan. In* Hyaluronan*; Kennedy, J. F., Phillips, G. O., Williams, P. A., Hascall, V. C., Eds.; Woodhead Publishing Ltd.: Cambridge, 2002; Vol. 1, pp. 75–78. Copyright 2002, Woodhead Publishing Ltd.*

Table 1 Example Dimension of Ball-Like HA Chains in Physiological Saline Solution

M	L (nm)	$[\eta]$ (cm^3/g)	V_s (cm^3/g)	$\langle r^2 \rangle^{1/2}$ (nm)	c, for Coil Overlap (μg/cm^3)
1×10^5	250	290	120	52	8600
5×10^5	1250	1100	420	140	2400
1×10^6	2500	1800	730	210	1400
3×10^6	7500	4400	1800	400	570
6×10^6	15,000	7700	3100	600	320

Adapted from Cowman, M. K.; Matsuoka, S. The Intrinsic Viscosity of Hyaluronan. In *Hyaluronan*; Kennedy, J. F., Phillips, G. O., Williams, P. A., Hascall, V. C., Eds.; Woodhead Publishing Ltd.: Cambridge, 2002; Vol. 1, pp. 75–78 with permission.

600 nm, which is far larger than compactly folded globular protein diameters of a few nm. The occupied space is filled with solvent, and the density of chain segments within the domain is low (AFM images show artificially broadened and exaggerated chain segment width due to probe tip profile), but the expanded coil domains start to interfere with each other at even low

concentration. The concentration at which chains would fill the solution and be forced to overlap domains is only 320 μg/cm^3 for the 6000 kDa HA. For comparison, the concentration of HA in synovial fluid is about 2500 μg/cm^3. Fig. 5 depicts a model for the crowding and overlapping of high-molecular-mass HA chains at such concentrations. The most important features of HA structure that lead to the low concentration for coil overlap are the naturally high molecular mass of HA and the chain stiffness leading to a large effective domain in solution.

The ability of polymers to crowd other macromolecules is explained by the theory for excluded volume. Ogston and Laurent[19,65–67] developed this theory to explain gel-filtration chromatography, in which the partition of globular proteins between a matrix containing randomly oriented rod-like polymers vs free solution determines the elution of the proteins from a column. The globular proteins can approach a segment of rod-like polymer until their surfaces touch, where the separation distance is equal to the sum of the radius of the sphere plus the radius of the cylindrical rod (Fig. 6). In an isolated polymer chain with an expanded coil conformation and a large hydrodynamic domain, the globular proteins can penetrate to the extent that they can find space between segments of the polymer chain. The available space decreases quickly as the density of polymer segments increases (Fig. 7) and is dependent on the size of the globular protein. A larger protein has a lower probability of finding space. The Ogston–Laurent expression for this probability of finding space is (Eq. 1)

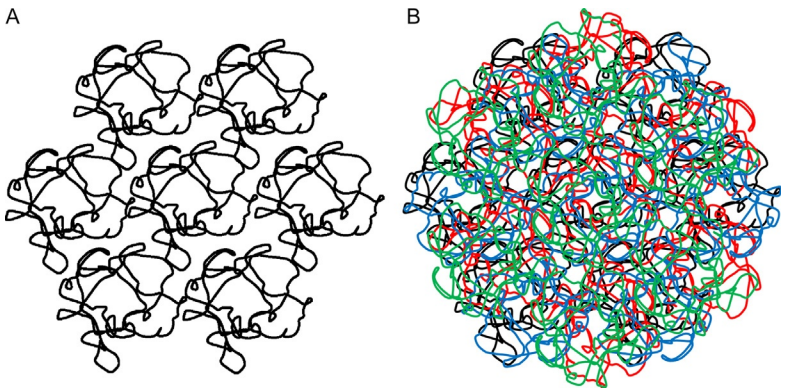

Fig. 5 Conceptual representation of coil overlap for 6000 kDa HA chains at (A) coil overlap point of approximately 320 μg/cm^3, where chains just touch, and (B) higher concentration of approximately 2500 μg/cm^3 as found in normal human knee joint synovial fluid.

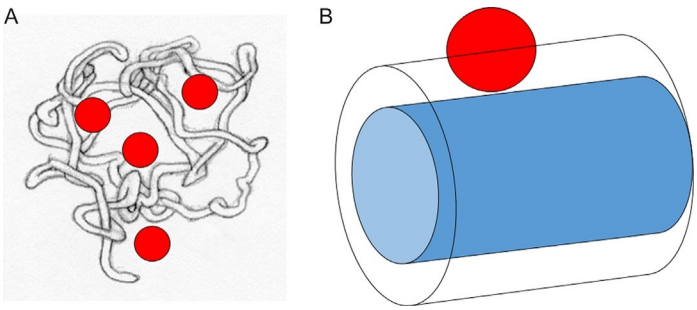

Fig. 6 Model for steric exclusion of a globular protein by an HA molecule. (A) The ability of small globular proteins to penetrate most of the hydrodynamic domain of an HA polymer. (B) The size of the excluded volume for a globular protein in the presence of a linear polymer as crowding agent. The cross-section of the cylindrical excluded domain has a radius equal to the sum of the radius of the crowding polymer and the thickness of a cylindrical shell determined by the radius of the globular protein. *This figure has been reproduced with permission from Cowman, M. K.; Hernandez, M.; Kim, J. R.; Yuan, H.; Hu, Y. Macromolecular Crowding in the Biomatrix. In* Structure and Function of Biomatrix. Control of Cell Behavior and Gene Expression*; Balazs, E. A., Ed.; Matrix Biology Institute: Edgewater, NJ, 2012; pp. 45–66. Copyright 2012, Matrix Biology Institute.*

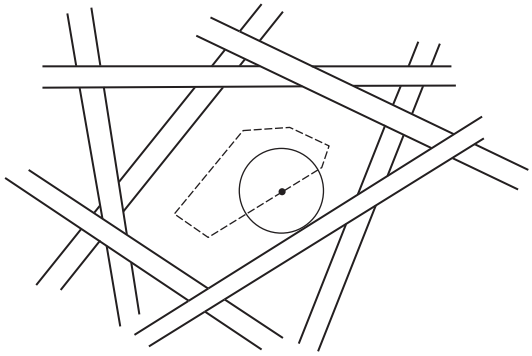

Fig. 7 Model proposed by Laurent for crowding of a spherical particle by a randomly oriented suspension of rods. The sphere is excluded from a cylindrical volume surrounding each rod, with radius equal to the sum of the rod and sphere radii. Overlapping of excluded volumes from multiple rods severely limits the space available to the sphere. *This figure has been reproduced with permission from Laurent, T. C. History of a Theory.* J. Chromatogr. A ***1993,*** 633*, 1–8. Copyright 1993, Elsevier Science.*

$$P = exp\left(-\pi L(r_s + r_r)^2\right) \tag{1}$$

where the probability P is exponentially decreased as the excluded volume (due to the volume occupied by the cylindrical rods of radius r_r and the

inaccessible shell around each rod, with a thickness determined by the radius r_s of the spherical protein probe) increases. A larger protein is excluded to a greater extent. The excluded volume increases with an increase in concentration of the polymer rods (L, length per unit volume), but does not depend on the length of individual rods or, equivalently, the molecular mass of polymers used to create the matrix.

The Ogston–Laurent excluded volume theory is extremely successful in understanding gel-filtration chromatography, but it is equally applicable to understanding the partition, stability, and interactions of proteins in physiologically important matrices. The equilibrium distribution of a globular protein between a matrix of polysaccharide (such as HA) or protein (such as collagen) polymers vs free solution is thus dependent on the mass concentration of the crowding polymers and the size (related to molecular mass) of the globular protein.[19] Excluded volume effects also alter protein association equilibria such that crowding favors associated forms.[20] If a native oligomer must be dissociated prior to fibrillar aggregation as occurs for some amyloid protein aggregation processes, the crowding effect disfavors the initial dissociation of native oligomers, but favors their subsequent aggregation into fibrils. Native protein folding is stabilized in the crowded intracellular and extracellular environments. Similarly, DNA denaturation and strand separation require an increase in volume, and crowding by added polymers therefore favors the native state.

The concept of excluded volume or macromolecular crowding can be generalized to the case of mutual crowding by identical polymers (Fig. 8). Matsuoka and Cowman[7,14,68–72] extended the expression (Eq. 1) of Ogston and Laurent for probability of finding space by considering the hydrodynamic volume occupied by all other polymer coils to be excluded to neighbor chains. In that case, the excluded volume can be expressed as the occupied volume fraction, ϕ, of the solution. From the Stokes–Einstein equation for the specific viscosity of a suspension of spheres, specific viscosity depends on the volume fraction as follows:

$$\eta_{sp} = 2.5\phi = c[\eta] \tag{2}$$

Because the specific viscosity of a dilute solution is equal to the product of the concentration, c, and the intrinsic viscosity, $[\eta]$, it follows that the occupied volume fraction can be expressed as $0.4c[\eta]$. Using that expression to replace the excluded volume term in the Ogston–Laurent equation (Eq. 1), the probability for a polymer coil to find space is

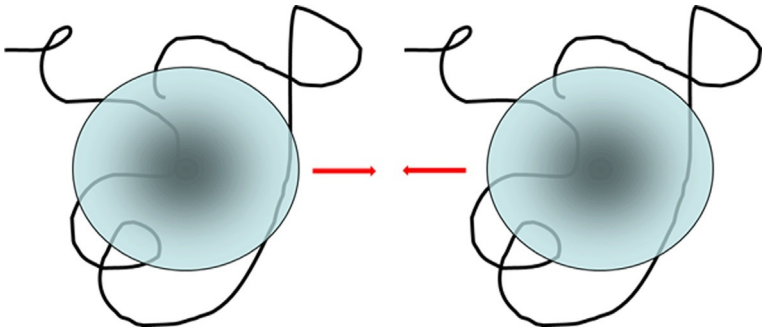

Fig. 8 Mutual crowding of HA molecules based on the effective hydrodynamic volume of each polymer being modeled as a sphere. *This figure has been adapted with permission from Cowman, M. K.; Hernandez, M.; Kim, J. R.; Yuan, H.; Hu, Y. Macromolecular Crowding in the Biomatrix. In* Structure and Function of Biomatrix. Control of Cell Behavior and Gene Expression*; Balazs, E. A., Ed.; Matrix Biology Institute: Edgewater, NJ, 2012; pp. 45–66. Copyright 2012, Matrix Biology Institute.*

$$P = exp(-\phi) = exp(-k'c[\eta])\ k' = 0.4 \tag{3}$$

The probability of finding space can also be expressed as the ratio of free volume to total volume and then further expressed in terms of the ratio of the real concentration to an effective concentration, c_{eff}, of polymer chains based on free space:

$$P = \frac{V_{free}}{V_{total}} = \frac{mass}{V_{total}} \times \frac{V_{free}}{mass} = \frac{c}{c_{eff}} \tag{4}$$

Since the effective concentration will determine the behavior of a crowded polymer solution, we now express the effective concentration in terms of the probability of finding space and the excluded volume

$$c_{eff} = \frac{c}{P} = c\,exp(k'c[\eta])\ k' = 0.4 \tag{5}$$

Eq. (5) states that the physicochemical properties of a polymer solution are subject to nonideality effects due to mutual macromolecular crowding when the effective concentration exceeds the real concentration due to volume exclusion or a reduction in available space. This concept provides a simple nonideality correction for analysis of data obtained by physicochemical methods such as viscosity, colloid osmotic pressure, and light scattering. Replacing c with c_{eff} in Eq. (2) yields:

$$\eta_{sp} = c_{eff}[\eta] = c[\eta]exp(k'c[\eta])\ k' = 0.4 \tag{6}$$

Expanded as a power series and truncating to keep only the first four terms, Matsuoka and Cowman proposed the semiempirical relation shown below:

$$\eta_{sp} = c[\eta]\left(1 + k'c[\eta] + \frac{(k'c[\eta])^2}{2!} + \frac{(k'c[\eta])^3}{3!}\right) \quad k' = 0.4 \tag{7}$$

A graph of Eq. (7) for polymer solution specific viscosity as a function of concentration and intrinsic viscosity (which reflects both polymer molecular weight and coil expansion) is shown in Fig. 9. If mutual macromolecular crowding were absent, the ideal behavior curve would be followed. In a real polymer solution, the nonideality contribution due to crowding causes a nearly exponential increase in specific viscosity as the overlap between polymer domains increases. Keeping the first four terms of the power series was proposed on the basis of the agreement with experimental observations for

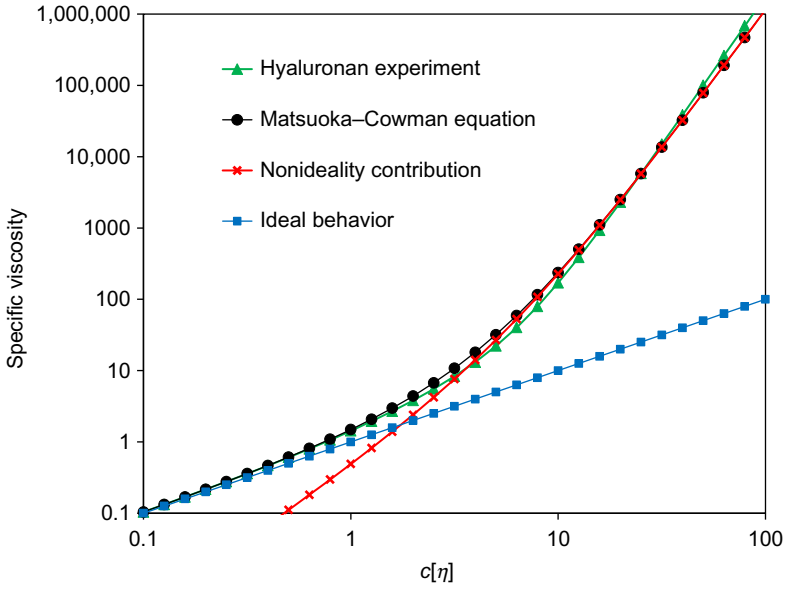

Fig. 9 The specific viscosity of HA, measured at low shear rate, depends on concentration and intrinsic viscosity in a predictable way. Experimental data for HA in physiological NaCl solution obtained by Berriaud and coworkers are well matched by the Matsuoka–Cowman equation. The equation is the sum of the contribution expected for an ideal dilute solution, and the nonideality contribution due to excluded volume. *This figure has been reproduced with permission from Cowman, M. K.; Schmidt, T. A.; Raghavan, P.; Stecco, A. Viscoelastic Properties of Hyaluronan in Physiological Conditions.* F1000Res ***2015,*** *4, 622. Copyright 2015, the authors.*

HA in neutral aqueous salt solution. Subsequently, the same equation was found to successfully match the specific viscosity behavior for multiple rigid, semiflexible, and flexible polymers in good solvents.[69] This shows that the behavior of HA is not unusual, except that the very high molecular mass of HA and the correspondingly large intrinsic viscosity cause the nonideality to be observed at relatively low concentrations. For example, the high viscosity of normal human knee joint synovial fluid reflects an HA concentration of ca. 2.5 mg/cm^3 and the ca. 6000 kDa average molecular mass for the HA (corresponding to an intrinsic viscosity of 7700 cm^3/g), for which the coil overlap parameter $c[\eta]$ would be 19 and the specific viscosity would be approximately 2100. As a comparison, a commercial preparation of HA for use in treatment of osteoarthritis pain might have HA with an average molecular mass of 1000 kDa and a concentration of 10 mg/cm^3, resulting in a coil overlap parameter of 18, closely similar to the normal synovial fluid HA.

A useful aspect of the mutual macromolecular crowding theory for viscosity is the ability to quantitatively relate specific viscosity of semidilute HA solutions to the concentration and intrinsic viscosity (and thus molecular mass) of the HA. Measurement of the specific viscosity at low shear rate (thus avoiding shear-induced distortion of the HA hydrodynamic shape and volume) for a semidilute HA solution of known concentration has been demonstrated to allow successful determination of HA molecular mass without extrapolating data to zero concentration.[73]

The effect of HA on tissue hydration via control of the colloid osmotic pressure is also well explained by the mutual macromolecular crowding theory. Substituting c_{eff} for c, the expression for osmotic pressure is given in Eq. (8):

$$\frac{\pi}{cRT} = \frac{1}{M} exp(k'c[\eta]) = \frac{1}{M} + \left(\frac{k'[\eta]}{M}\right)c + \left(\frac{(k')^2[\eta]^2}{2M}\right)c^2 + \ldots \; k' = 0.4 \quad (8)$$

A graph of the osmotic pressure for HA is shown in Fig. 10, with the predicted osmotic pressure due to crowding compared with experimental data obtained by Laurent and Ogston.[74] In this case the use of the first three terms of the nonideality correction matches the experimental data well. It is worth noting that the expanded expression for osmotic pressure resembles a virial expression with coefficients representing nonideality, because the mutual macromolecular crowding theory is essentially a theory for virial coefficients in polymer solutions. The prediction for the second virial coefficient contains the ratio $[\eta]/M$. Considering the $M^{0.80}$ dependence of the

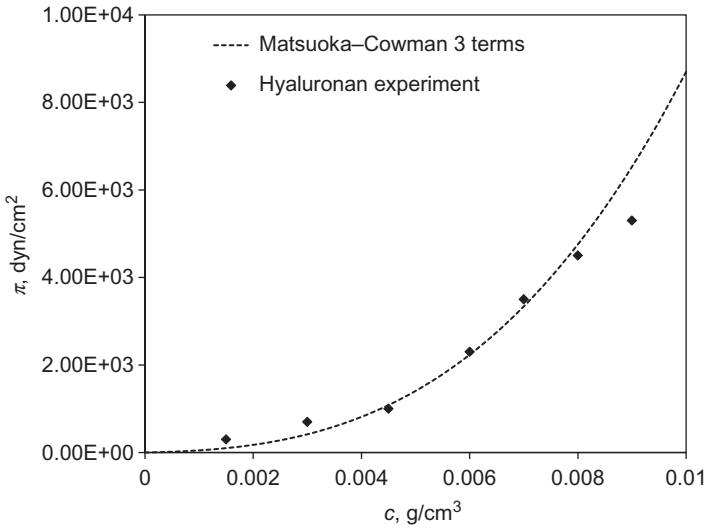

Fig. 10 Experimental colloid osmotic pressure for 1500 kDa HA in aqueous salt solution reported by Laurent is well matched by prediction from the Matsuoka–Cowman equation using the first three terms of the polynomial. *This figure has been adapted with permission from Cowman, M. K.; Matsuoka, S. Experimental Approaches to Hyaluronan Structure.* Carbohydr. Res. ***2005,*** 340*, 791–809. Copyright 2005, Elsevier Ltd.*

intrinsic viscosity for HA, the virial coefficient is predicted to depend on $M^{-0.20}$, which has been experimentally confirmed.[50] Light-scattering data extrapolated to zero angle can similarly be corrected for nonideality due to crowding.[71]

An interesting aspect of the mutual macromolecular crowding theory is the evident connection between the thermodynamic properties of osmotic pressure and light scattering with the hydrodynamic properties of polymer solution viscosity.

The relaxation time of a polymer chain is another measure of its size, expressed as $[\eta]M$, the molar volume. It is also affected by the effective viscosity of the local environment through which the chain moves, and therefore by crowding.[71] A long relaxation time causes shear thinning, a reduction in the solution viscosity when chain rearrangement is slow relative to distortion (chain extension) caused by shearing (Fig. 11). It also causes a transition from viscous to elastic behavior under cyclic distortion as a function of increasing rate of change (Fig. 12).[75] The effect of increased local viscosity due to crowding on relaxation time for a polymer is expressed in terms of an effective viscosity, as follows:

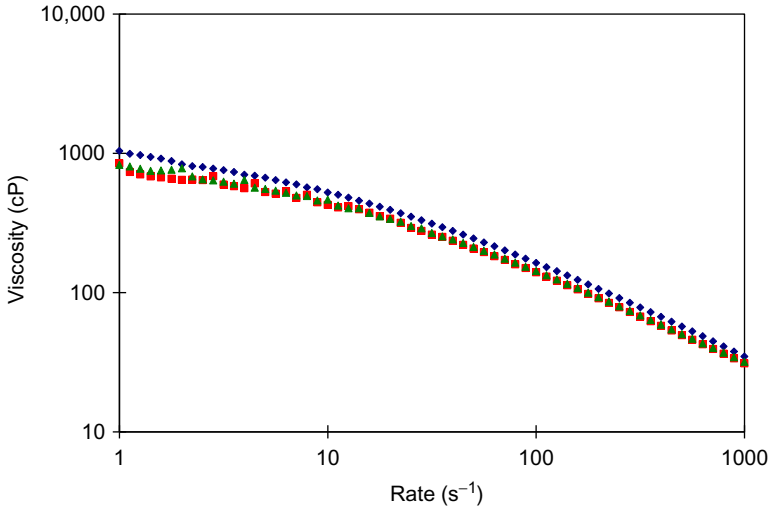

Fig. 11 Shear rate dependence of the viscosity of a polydisperse HA sample with viscosity-average molecular mass of 1700 kDa at a concentration of 5 mg/cm^3 in physiological saline at 25°C. Data from three consecutive runs are shown. *This figure has been reproduced with permission from Cowman, M. K.; Chen, C. C.; Pandya, M.; Yuan, H.; Ramkishun, D.; LoBello, J.; Bhilocha, S.; Russell-Puleri, S.; Skendaj, E.; Mijovic, J.; Jing, W. Improved Agarose Gel Electrophoresis Method and Molecular Mass Calculation for High Molecular Mass Hyaluronan.* Anal. Biochem. ***2011,*** 417, *50–56. Copyright 2011, Elsevier Inc.*

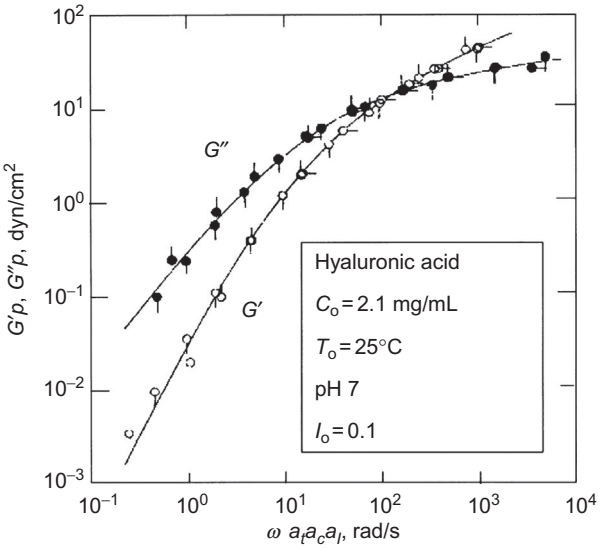

Fig. 12 Master curves for the elastic modulus (G') and the viscous modulus (G'') of a solution of 2800 kDa HA, as a function of the frequency of displacement. *This figure has been reproduced with permission from Gibbs, D. A.; Merrill, E. W.; Smith, K. A.; Balazs, E. A. Rheology of Hyaluronic Acid.* Biopolymers ***1968,*** 6, *777–791. Copyright 1968 John Wiley and Sons Inc.*

Table 2 Matsuoka–Cowman Predicted Scaling Factors for HA in Semidilute Saline Solution: Comparison With Experiment

Property	Scaling Factors in Semidilute Solution: Predicted (for Hyaluronan, $[\eta] \propto M^{0.80}$)	Scaling Factors in Semidilute Solution: Experiment	Hyaluronan Experiment References
Specific viscosity	$c^4[\eta]^4$ $(=c^4M^{3.2})$	$c^{3.8–4.1}M^{3.3–4.0}$	76–82
Relaxation time	$c^2[\eta]^3M$ $(=c^2M^{3.4})$	c^2M^3	81,82
Elastic modulus	$c^2[\eta]M^{-1}$ $(=c^2M^{-0.2})$	$c^{2.0–2.8}M^0$	81,82
Second virial coefficient	$[\eta]M^{-1}$ $(=M^{-0.2})$	$M^{-0.19}$	50

Reproduced from Cowman, M. K. Mutual Macromolecular Crowding as the Basis for Polymer Solution Non-ideality. *Polym. Adv. Technol.* **2017,** *28*, 1000–1004 with permission

$$\tau \propto \frac{\eta_0}{RT}[\eta]M(exp(k''c[\eta])) \tag{9}$$

and expansion of the exponential term as a power series gives

$$\tau \propto \frac{\eta_0}{RT}\left([\eta]M + k''c[\eta]^2M + \frac{(k'')^2}{2!}c^2[\eta]^3M + \ldots\right) \tag{10}$$

For a semidilute HA solution, the third term is a good match for the concentration and molecular mass dependence of the relaxation time as measured by shear thinning or the deformation rate for the transition from viscous to elastic behavior (Table 2).[50,76–82] Furthermore, because the elastic modulus, G_e, is equal to the viscosity divided by the relaxation time, the mutual macromolecular crowding theory also allows prediction of the elastic modulus dependence.

4. HA SELF-ASSOCIATION

The observation of a double helical form of HA in the solid state by X-ray diffraction suggests that HA chains can have mutual affinity, at least under unusual ionic conditions. Furthermore, as shown in Fig. 2, HA deposited on mica or graphite surfaces has a strong tendency for self-association. Multistranded cable-like aggregates are frequently observed, especially if oriented by flow during deposition or if exposed to air.

In contrast, the equilibrium state of well-dissolved high-molecular-mass HA in neutral aqueous salt solutions in vitro and in biological fluids in vivo

does not show evidence for the presence of aggregates or intermolecular self-association. The physicochemical properties related to rheology, osmotic pressure, and light scattering can be quantitatively matched by the simple theory for mutual macromolecular crowding of independent molecules (Figs. 9–12 and Table 2).[7,71] Similarly, measurements of the diffusion coefficient of HA by boundary relaxation in an ultracentrifuge,[83] or under quiescent conditions by confocal fluorescence recovery after photobleaching (confocal FRAP)[84,85] fit a model for semidilute polymer solution behavior without any evidence for chain–chain association.

The situation is less clear for low-molecular-mass HA, corresponding to HA less than about 40 kDa, which adopts a more rod-like conformation in dilute solution (Fig. 4). There have been numerous reports that solutions of low-molecular-mass HA are prone to aggregation,[58,62] and substantial losses can occur on filtration. Evidence that short HA chains can easily aggregate in 0.15 M NaCl solution (but not in 0.15 M KCl solution) has been obtained by light scattering and other methods.[86]

These apparently conflicting observations can be rationalized in terms of a weak, enthalpically favorable affinity of HA chains for each other in physiological saline solution, offset by the entropic loss accompanying association. For high-molecular-mass HA in solution, considerable configurational entropy would be lost by adoption of the fibrillar aggregates. For rod-like short HA chains, the entropic penalty for association is lower, and association is more favorable.

Protein binding to HA in vivo can tip the balance toward self-association. HA assembles into cables/fibers in tissues under inflammatory conditions in which HA content is significantly increased relative to that of the normal condition.[87–91] HA–protein interactions are critical to the formation of these fibrillar assemblies. The protein TSG-6 binds noncovalently to HA,[92–94] and dimerization of TSG-6 can link HA chains together.[95,96] TSG-6 also catalyzes covalent modification of HA by transfer of the heavy chains of IαI,[97–101] and those heavy chains self-associate to link HA chains together.[102,103] HA-binding proteoglycans such as versican may also be included in the fibrillar assemblies.[90]

5. HA SIZE AND WHY IT MATTERS

In vivo, the extracellular matrix is continually modified by synthesis, degradation, and removal by transport of its protein and glycosaminoglycan (GAG) components. It is not a static environment. Changes in the content,

size, and composition of the GAGs have been found to influence such processes as development, aging, inflammation, tissue repair, and disease initiation and progression.

5.1 High-Molecular-Mass HA Is the Physiological Protector of Cells

There are three known hyaluronan synthase enzymes, HAS1, HAS2, and HAS3.[4] The enzymes are localized in the plasma membrane and directly export the growing HA chain to the extracellular environment. All three enzymes are capable of synthesizing high-molecular-mass HA (up to about 1000 kDa), but only HAS2 has been reported to be able to synthesize HA as large as 6000 kDa, which is the most commonly reported average size for newly synthesized HA found in healthy tissues.[104,105]

At the cell surface, HA is noncovalently bound to the integral membrane receptor protein CD44.[106–110] The intrinsic binding affinity between HA and CD44 is relatively low, but a single high-molecular-mass HA chain can bind multiple CD44 proteins simultaneously.[111,112] This higher affinity multivalent interaction results in clustering of CD44 proteins.[113] (HA chains that are linked into aggregates by virtue of binding to TSG-6 dimers or modification by the dimerizing heavy chains of IαI have further enhanced binding affinity for CD44.[95,96,103,114] A similar observation has been made for HA binding to LYVE-1, an HA receptor found on lymphatic endothelial cells.[115]) CD44-tethered HA serves as a scaffold for assembly of proteoglycans such as versican, as well as other HA-binding proteins. The proteoglycans have additional binding interactions with multiple proteins. The net effect of the multiplicity of interactions is the creation of a complex pericellular matrix network.

As is predicted by the theory for mutual macromolecular crowding, the presence of high-molecular-mass HA and other large macromolecular complexes at the cell surface affects the biomechanical and osmotic properties of the pericellular matrix. The excluded volume effect controls/reduces the equilibrium concentration of proteins near the cell surface and alters association equilibria, favoring greater association and more compact structures. The HA-based matrix further acts as a protective alternate target for reactive oxygen and nitrogen species (ROS/RNS) generated during inflammation and limits penetration of those species to the cell membrane.

Cell-signaling pathways are highly dependent on the status of the pericellular matrix and the HA component. CD44 clustering in the presence of high-molecular-mass HA activates protective signaling. This is true for both

normal and tumor cells.[21,116] The presence of high-molecular-mass HA provides a protective coat for the cell.

Under stress due to injury, infection, or sterile inflammation, the HA synthase enzymes can be upregulated and activated, resulting in increased levels of HA. This is a defense mechanism but, in excess, can have multiple consequences. Excess HA, especially when bound to proteins such as TSG-6 and the heavy chains of IαI, can aggregate into cable-like fibrillar assemblies that must be eliminated before inflammation can be fully resolved.[8]

Excess HA also drives the formation of microvilli that extend from the cell surface and shed microvesicles into the extracellular matrix.[18,117–121] These HA-coated plasma membrane-derived extracellular vesicles can carry nucleic acids and proteins to other cells. The role of increased HA synthesis in cell–cell communication, especially in relation to creation of the tumor microenvironment, is only beginning to be revealed. We propose that the driving force for the formation of the microvilli is the dramatic increase in osmotic pressure associated with high HA concentration, as predicted by mutual macromolecular crowding theory. Transport of water across the cell membrane to the HA matrix shrinks the cell volume slightly relative to the available plasma membrane surface, and this may directly result in the formation of microvilli.

The defensive excess production of HA has a metabolic cost. Cells that produce HA at a high rate can deplete stores of glucose and UDP-GlcNAc. (The reverse is also of interest—excess glucose can be reduced by the increased synthesis of HA.[122–124]) Where high levels of HA have been associated with pathological states, it is important to note that HA may not be a base cause of the pathology, but that the defensive process of producing it at high levels may lead to a weakened state. Exogenous HA used therapeutically may be helpful in reducing the metabolic burden associated with cell-surface protection.

5.2 Low-Molecular-Mass HA Stimulates Defensive Cellular Responses

Because high-molecular-mass HA represents the protective homeostatic state, any process that degrades HA may stimulate a response. HA degradation by enzymatic or nonenzymatic mechanisms results in the presence of HA fragments. A great deal of interest now surrounds low-molecular-mass HA.[6,8,9,21–24,125–133] The fragments of HA have been widely reported to signal both directly and indirectly via cell-surface receptor proteins such as CD44, RHAMM, TLR2, TLR4, and MD-2. HA-mediated CD44

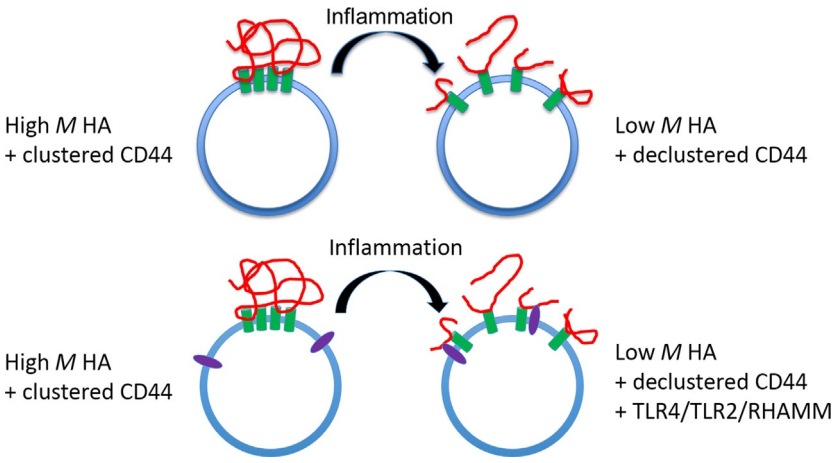

Fig. 13 The clustering of CD44 receptors at the cell surface is disrupted when HA is degraded under inflammatory conditions. The cell signaling of CD44 can be altered by declustering, and also by its increased availability for interaction with other receptor proteins such as RHAMM, TLR4, and TLR2.

clustering has been shown to be disrupted when HA size is reduced. The declustered state affects CD44 interactions on the cytoplasmic face of the plasma membrane, but it also may be permissive for extracellular face CD44 interactions with other cell-surface receptor proteins (Fig. 13). There is some disagreement in the literature regarding whether HA fragments can bind directly to TLR2 or TLR4, or whether they signal through the TLRs by a secondary mechanism such as CD44 declustering. By either mechanism, the presence of HA fragments has been proposed to act as a danger signal. The signaling can lead to the expression of inflammation mediators and poorly controlled chronic inflammation. Alternatively, it can lead to defensive cellular responses mediated by the TLRs. This issue is far from settled, because HA fragments do not always have proinflammatory or other signaling effects, and the medical use of hyaluronidase enzyme does not cause an inflammatory response.[134–136]

5.3 Mechanisms for HA Degradation

5.3.1 Hyaluronidases

Two hyaluronidases found in vertebrates, Hyal1 and Hyal2, have long been considered the primary degradative enzymes for HA, but both have acidic pH optima.[137,138] HA must be internalized by cells for degradation by Hyal1 in lysosomes. Hyal2 has often been cited as the principal cell-surface

degradative enzyme for HA in most tissues. GPI-anchored Hyal2 is found colocalized with CD44 at the cell surface in lipid rafts[139–141] and can be shed into the extracellular environment.[142] It has only weak activity at neutral pH, but may function at the cell surface when colocalized with NHE1, which acidifies the local microenvironment at the surface of tumor cells.[143] Both Hyal1 and Hyal2 are endoglycosidases, catalyzing random hydrolytic cleavage of the β-(1→4)-glucosaminidic linkages of HA. Increased expression of Hyal2 has been observed in many pathological conditions.

Recently, two other proteins have been identified that may play the most critical roles in degradation of tissue HA. CEMIP, also called KIAA1199 or HYBID, is an HA-specific binding protein that has not been shown to directly cleave HA, but is active in HA degradation by a mechanism that appears to involve HA internalization via the clathrin-coated pit pathway of live cells.[144–146] TMEM2 is a newly discovered integral membrane protein that acts as an HA-specific hyaluronidase with a pH optimum of about 6–7.[147] It can degrade high-molecular-mass HA into small fragments. This enzyme now appears most likely to be the primary degradative enzyme for extracellular HA, reducing its size prior to internalization for complete degradation in the lysosomes.

PH-20 hyaluronidase, also called SPAM1, is known as the testicular hyaluronidase, although it can be expressed at low levels in other tissues. It is a GPI-anchored protein and is active at neutral pH.[148–150] Recombinant human PH-20 (rhPH-20) has been commercialized for medical use, primarily to enhance delivery of chemotherapeutic agents by degrading HA, which surrounds tumor cells and exerts a high osmotic pressure causing compression of blood vessels.[151,152] The same preparation of rhPH-20 has also been reported to be of value in improving mobility for patients with severe muscle stiffness following cerebral injury where the PH-20 may function by disrupting gel-like HA and HA–protein deposits that can build up and reduce sliding between layers of the fascia in muscle.[14,153]

5.3.2 Degradation of HA by ROS/RNS

HA is susceptible to degradation by hydroxyl radicals, peroxynitrite, and hypochlorite anion, all of which can be created in vivo and are increased during inflammation.[138,154,155] A valuable function of HA is the protection of cellular proteins, lipids, and nucleic acids from ROS/RNS by acting as an alternate target and limiting penetration of the reactive species to the cell surface. Inflammation is therefore associated with the potential for reduction in HA molecular mass, and the production of bioactive "danger signal"

fragments. The effects of ROS and RNS on HA are also of interest with respect to the isolation and purification of HA in laboratory environments. Therapeutic HA production must be performed under conditions that minimize HA degradation. Similarly, analysis of tissue HA size can only be accurate when the HA size is not decreased by degradation during purification and analysis.

Mechanisms for production of ROS/RNS in biological systems have been reviewed by Halliwell and Gutteridge[156,157] and are briefly summarized here.

Hydroxyl radicals. In the presence of iron(II) or copper(I), hydroxyl radicals can be created from hydrogen peroxide by the Fenton reaction[156–160]:

$$Fe^{2+} + H_2O_2 \rightarrow Fe^{3+} + OH^- + {}^{\bullet}OH$$

In this reaction, iron (or copper) can be catalytic. The oxidized Fe^{3+} can be reduced back to Fe^{2+} by reaction with superoxide anion ($O_2^{-\bullet}$):

$$Fe^{3+} + O_2{}^{-\bullet} \rightarrow Fe^{2+} + O_2$$

Alternatively, Fe^{3+} can be reduced to Fe^{2+} by additional hydrogen peroxide:

$$Fe^{3+} + H_2O_2 \rightarrow Fe^{2+} + O_2{}^{-\bullet} + 2H^+$$

Fe^{3+} can also be reduced to Fe^{2+} by ascorbic acid and other species, including hydroquinone, merthiolate, sodium dithionite, dihydroxymaleate, nitric oxide, and cysteine or proteins containing cysteine in the reduced state. Photochemical reduction of iron complexes has also been reported.

Iron chelators can have either positive or negative effects on the ability of iron to cause the formation of ROS. When the effect is to increase ROS production, it may derive from an increase in solubility of iron in the solution. This effect has been reported for EDTA[161,162] and even phosphate anion. EDTA has also been reported to form a photoreducible complex with Fe^{3+}. Other chelators sequester the iron and make it unable to participate in ROS production. These include deferoxamine, bathophenanthroline, and diethylenetriaminepentaacetic acid (DETAPAC). These latter agents are highly valuable additives for isolation of intact HA.[163]

The source of the iron can be impurities in the solution associated with contact with metal, or the iron can be liberated in tissues from degraded heme or ferritin.[159,161,164] The source of superoxide anion in biological

systems is activated PMNs (polymorphonuclear leukocytes).[165] Dismutation of two superoxide anions can create hydrogen peroxide. Hydrogen peroxide can also be created by photochemical means.

In the absence of transition metal ions, hydroxyl radicals may be generated from superoxide anion by superoxide dismutase of activated PMNs, creating hydrogen peroxide,[166] followed by further reaction of hydrogen peroxide with superoxide anion by the Haber–Weiss reaction, although the relevance of this latter reaction to physiological conditions has been questioned,[157] and myeloperoxidase and catalase can scavenge hydrogen peroxide[167]:

$$O_2^{-\bullet} + O_2^{-\bullet} + 2H^+ \rightarrow O_2 + H_2O_2$$
$$O_2^{-\bullet} + H_2O_2 \rightarrow O_2 + OH^- + {}^{\bullet}OH$$

Hydroxyl radicals can be scavenged by a large number of agents including mannitol, thiourea, uric acid, and dimethyl sulfoxide.

The degradation of HA by hydroxyl radicals and its protection by free-radical scavengers are well documented.[52,167–191] The fragmentation reaction occurs randomly. Not only are glycosidic linkages cleaved, but there is the possibility of other structural changes including ring opening. Thus, HA fragments that are generated by ROS may not have the same biological effects as HA fragments created by enzymatic cleavage.[190]

Peroxynitrite. Peroxynitrite can be generated by reaction of nitric oxide, produced by the nitric oxide synthase enzymes (NOS), with superoxide anion, released by activated PMNs[192–194]:

$$NO^{\bullet} + O_2^{-\bullet} \rightarrow ONOO^-$$

The pK_a of peroxynitrite is about 6.8,[195,196] resulting in formation of peroxynitrous acid, the reactivity of which suggests formation of hydroxyl radicals by homolytic fission,[197,198] although this is disputed and an alternate mechanism involving a vibrationally excited state that acts as if it has two radical ends has been proposed[199–201]:

$$ONOO^- + H^+ \rightarrow ONOOH \rightarrow ONO^{\bullet} + {}^{\bullet}OH$$

Increased expression of NOS is common in inflammatory disease processes. Our laboratory was the first to demonstrate degradation of HA by peroxynitrite, and this has subsequently been reaffirmed by several groups.[155,202–204]

Hypochlorite ion. Hypochlorite ion can be generated by myeloperoxidase enzymes of PMNs[205]:

$$H_2O_2 + Cl^- \rightarrow OCl^- + H_2O$$

Methionine blocks this reaction. Hypochlorite anion may function by participating in production of hydroxyl radicals.[182] HA degradation by hypochlorite ion has been documented.[205–207]

5.3.3 Degradation of HA by Other Chemical and Physical Means

HA can be hydrolyzed in acid or alkali.[208–212] HA can be degraded by heating under pressure, complicating sterilization in an autoclave,[59] but solutions of HA in physiological saline are stable under boiling for 30 min.[73] Over longer time periods at elevated temperature, HA can be degraded in solution or in the solid state.[213,214]

HA chains can be broken by physical shearing and sonication.[215–218] HA can also be degraded by freeze-drying,[219] although this may require the presence of the free acid form.[220,221]

HA can be degraded by short-wavelength UV (ca. 185–300 nm) irradiation,[222,223] although it is stable to sunlight (with a lowest wavelength at the earth's surface of about 292 nm), unless in the presence of ozone.[224] HA is also degraded by pulse radiolysis with high-energy electrons, produced by gamma irradiation,[177,225,226] and by exposure to X-ray radiation at doses relevant to radiotherapy.[227]

6. EXPERIMENTAL DETERMINATION OF HA CONTENT AND SIZE IN VIVO

Because the content and size of HA can have important effects on normal and pathological processes, there has been strong interest in documenting those factors. The goal is to leverage that knowledge to develop diagnostic and therapeutic approaches to disease management. Here we describe the methods used to obtain that data and then summarize some relevant findings.

6.1 Isolation Methods

The isolation of HA is most commonly performed by processes that are based on the techniques historically used for extraction and purification of DNA[228,229] because glycosaminoglycans are polyanions with solubility properties that are qualitatively similar to DNA and RNA. The key steps

in those DNA isolation procedures are (1) denaturation and removal of protein, for example, by shaking/mixing with chloroform and subsequent centrifugal separation of aqueous and organic layers, and (2) precipitation of DNA with ethanol or acetone. Thus, Balazs in his 1979 US Patent[230] isolated ultrapure hyaluronan (HA) from rooster comb by a method that closely mimicked the older DNA isolation methods.

In current protocols for isolation of HA from solid tissues,[126,163,231–236] the protein denaturation and removal step with chloroform is commonly replaced or augmented by proteolytic digestion. Lipid removal may be accomplished by initial defatting of the tissue in acetone and ethanol. To remove DNA and RNA, enzymatic degradation of nucleic acids is commonly employed. Thus, multiple enzymatic digestions and solvent changes with removal of low-molecular-mass components by dialysis or precipitation are required. Isolation of HA from native biological fluids or cell culture conditioned medium follows similar steps.[24,104,125,237,238]

Our current laboratory protocols[24,125,126] (Fig. 14) for isolation of intact HA from skin or milk usually involve overnight protease digestion, multiple $CHCl_3$ extractions, two overnight dialysis steps, and two overnight ethanol precipitations. Even after all these steps, impurities remain. Further purification using anion-exchange chromatography on spin columns eluted with a step gradient of NaCl, followed by dialysis and drying by centrifugal evaporation (or ethanol precipitation), and redissolution are employed.

Because HA is highly susceptible to degradation by hydroxyl radicals generated in the presence of trace levels of contaminating Fe(II) or Cu(I), and this problem is exacerbated by the presence of ascorbic acid or other redox-active molecules that can regenerate the active metal ion species, HA isolation is best performed in the presence of an effective chelator such as deferoxamine, but not EDTA.

6.2 Specific Quantification Methods

If quantification of HA and other GAGs is desired, but the polymers do not need to be left intact, isolation protocols are followed by enzymatic degradation to disaccharides or small oligosaccharides, then chromatographic, electrophoretic, and/or mass spectrometric analysis can be employed.[239–251] These methods are sensitive and quantitative.

Specific quantification of intact HA polymers in the presence of remaining impurities can be accomplished by ELISA or ELISA-like assays.[231,234,237,252–264] Because there is no antibody for HA, these assays

Example HA Isolation Protocol for 7–10 mL Milk

Note: Spiking fluid or solid tissues with monodisperse HA (also acts as a carrier) before isolation can check for HA degradation during isolation.

1. To remove lipids, put 7–10 mL milk in a 15-mL centrifuge tube. Centrifuge at 4000 × *g*, 5 min. Place tube in freezer for 2 h to solidify the layers. Remove from freezer and scoop out the lipid layer while the aq layer is still frozen.
2. Add ca. 200 μL of proteinase K stock solution (25 μg/μL) to make the final concentration 1 μg/μL. Incubate 65°C overnight.
3. Centrifuge 4000 × *g*, 5 min; keep aq layer. (Remove last of lipid layer.)
4. Dialyze vs 2 L H_2O overnight using a 10-mL 2 kDa MWCO dialysis membrane. Change H_2O 2× during first 4 h.
5. Concentrate to 400 μL by centrifugal vacuum concentrator.
6. Fractionate on strong anion-exchange mini spin column, wash with 0.1 M NaCl and 0.2 M NaCl, then elute HA with 0.4 M NaCl followed by 0.7 M NaCl (or 0.7 M NaCl, only. Sulfated GAGs elute at >1 M NaCl.)
7. Remove NaCl by dialysis against 1–2 L H_2O overnight, changing H_2O 2× during first 4 h, or by precipitating HA with 4 vol ethanol.

Example HA Isolation Protocol for 60–100 mg Skin

Note: Spiking fluid or solid tissues with monodisperse HA (also acts as a carrier) before isolation can check for HA degradation during isolation.

1. Add 400 μL of 0.15 M Tris pH 8.3, 0.15 M NaCl, 0.01 M $CaCl_2$, 5 mM deferoxamine mesylate, 0.1% SDS, 7 U proteinase K/mg tissue; incubate 55°C overnight.
2. Centrifuge 18,000 × *g*, 5 min; keep supernatant.
3. Add NaCl to 2 M.
4. Add equal vol $CHCl_3$ and shake.
5. Centrifuge 18,000 × *g*, 10 min; keep upper aq layer.
6. Dialyze to 0.1 M NaCl, 2 h, using MINI dialysis units 7000 MWCO.
7. Precipitate HA with 4 vol ethanol overnight at −20°C.
8. Centrifuge 18,000 × *g*, 20 min; keep pellet.
9. Dissolve in 100 μL of 50 mM Tris pH 8, 20 mM NaCl, 50 U Benzonase; incubate 37°C for 4 h.
10. Repeat steps 3–8.
11. Dissolve in 30 μL H_2O.
12. Optionally, boil to denature any remaining protease, then repeat steps 9–11.
13. Add H_2O and 2 M NaCl to make 400 μL in 0.1 M NaCl.
14. Fractionate on strong anion-exchange mini spin column, washing with 0.2 M NaCl (removes junk), then elute HA with 0.7 M NaCl (sulfated GAGs elute at >1 M NaCl).
15. Remove NaCl by dialysis or by precipitating HA with 4 vol ethanol.

Fig. 14 Example HA isolation protocols for use with biological fluids or solid tissues.

are based on the use of HA-specific binding proteins. For example, the aggrecan proteoglycan binds HA highly specifically. Either the intact proteoglycan or a terminal fragment called G1-IGD-G2, often referred to as HA-binding protein (HABP), may be used. The Link protein, also called CRTL1 or HAPLN1, and several other HA-specific proteins are similarly useful. The assay format is usually microplate-based and can be a sandwich or competitive type.

Sandwich ELISA-like assays for HA may have HABP or other specific binding protein immobilized on a surface to which HA in a sample can bind.

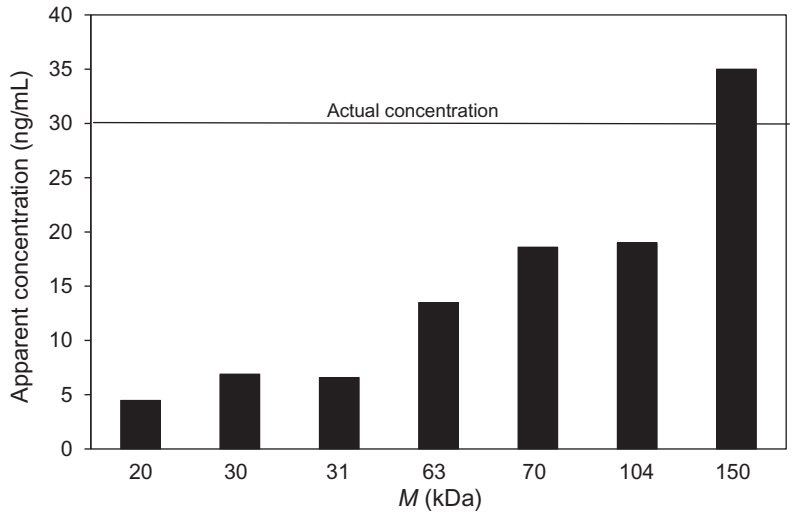

Fig. 15 HA detection by a commercial ELISA kit employing sandwich assay format is inaccurate for low-molecular-mass HA. The apparent concentration measured for different HA samples with an actual concentration of 30 ng/mL (*horizontal line*) depends on HA size, below about 150 kDa. Short HA chains bound to a surface are difficult to probe with a specific detector protein. *This figure has been adapted with permission from Yuan, H.; Tank, M.; Alsofyani, A.; Shah, N.; Talati, N.; Lobello, J. C.; Kim, J. R.; Oonuki, Y.; de la Motte, C. A.; Cowman, M. K. Molecular Mass Dependence of Hyaluronan Detection by Sandwich ELISA-Like Assay and Membrane Blotting Using Biotinylated Hyaluronan Binding Protein.* Glycobiology ***2013,*** *23, 1270–1280. Copyright 2013, the authors.*

Bound HA is detected by addition of suitably labeled detector protein, such as biotinylated HABP, that can be quantified by addition of streptavidin conjugated to an enzyme reporter. The sensitivity of sandwich assays is high, with a detection limit as low as 0.05 ng of HA. Unfortunately, the sandwich assay format poorly detects HA with molecular mass less than about 150 kDa[262,263] (Fig. 15). This phenomenon has been attributed to uninterrupted binding of short HA chains to the surface without formation of loops that are required for accessibility to the biotinylated detector protein.

Competitive ELISA-like assays are preferred for detection of HA, because the HA–protein binding step occurs in solution rather than at a surface. Unbound HABP is detected by its binding to HA or an antibody on a surface. In competitive ELISA-like assays, HA ranging in size from that of a long polymer to a decasaccharide (the minimum size for binding of HA to HABP) is detected equally, but the sensitivity is usually lower than that of sandwich assays, with reported detection limit in the competitive assays being about 1 ng.

6.3 Methods for Molecular Mass Analysis

Commonly employed physicochemical methods to analyze average molecular mass and molecular mass distribution require HA to be nearly pure and dissolved in a neutral aqueous salt solution (usually NaCl) with an ionic strength of at least 0.1.[72] The weight-average molecular mass can be determined by light scattering using data extrapolated to zero angle and zero concentration. A closely similar viscosity-average molecular mass can be obtained by determination of intrinsic viscosity measured at, or extrapolated to, low shear rate. As we have seen above (Fig. 9), it is also possible to determine viscosity-average molecular mass from low-shear viscosity data for a semidilute solution of known concentration using the nonideality correction predicted by mutual macromolecular crowding theory.[73] For determination of HA molecular mass distribution, a method for fractionation of the HA by molecular mass is coupled with concentration determination and light scattering or viscosity analysis. SEC–MALLS (size-exclusion chromatography with multiangle laser light scattering) is widely used to analyze HA samples in which the molecular mass ranges up to about 2000–5000 kDa, depending on the chromatographic column separation range.[72,265] In choosing the appropriate columns, it is important to bear in mind that the expanded coil conformation of HA occupies a much larger hydrodynamic volume than a globular protein of the same molecular mass, and nonideality effects can be significant at even low concentration.

The physicochemical methods have been successfully applied to the analysis of HA in synovial fluid, where the concentration is high, ca. 2–3 mg/mL, and purification from contaminating globular proteins and small molecules is easily accomplished. In other fluids and tissues, the levels of HA are lower, and purification is often incomplete. The most commonly used methods for analysis of HA isolated from fluids and tissues are based on chromatographic or gel electrophoretic separation of HA by size, followed by sensitive or specific quantification. Size-exclusion chromatography can be coupled with detection by labeled HA-specific binding protein, or with detection by an ELISA-like assay.[233,266–269] The columns must be precalibrated with HA samples of low polydispersity and known average molecular mass determined by a primary method such as light scattering. Gel electrophoretic separation methods similarly require coelectrophoresis of HA standards with known molecular mass and low degree of polydispersity.[2,73,163,270,271] If the HA sample is nearly pure, or contaminated only

with molecules not bound to HA and having sufficiently different electrophoretic mobility, gels can be stained with a dye such as Stains-All, and densitometric scans can be used to determine HA molecular mass distribution and calculate weight- and number-average molecular mass. Alternatively, blotting or electrophoretic transfer of the separated HA to a positively charged nylon membrane allows specific detection of HA with a labeled binding protein.[270] Unfortunately, HA attachment to the cationic surface limits accessibility to detector proteins, and blotting methods do not accurately detect HA with a molecular mass of less than about 150 kDa.[263]

The choice of gel matrix for electrophoretic separation of HA is dictated by the size range of interest.[73,271] Agarose gels containing 0.5% agarose in Tris–acetate–EDTA (TAE) buffer can be used to separate HA from about 200 kDa to over 6000 kDa. The electrophoretic mobility is linearly related to the logarithm of the HA molecular mass, and densitometric scans of stained gels allow accurate determination of molecular mass distribution and weight-average molecular mass. Fig. 16 shows the electrophoretic separation of two polydisperse commercial samples of pure HA on 0.5% agarose in TAE. The coelectrophoresed HA standards were nearly monodisperse chemoenzymatically synthesized HA (Select-HA™), for which the HA molecular masses were determined by SEC–MALLS. Fig. 17 shows the molecular mass distribution of the polydisperse HA obtained from the densitometric scan using the HA standards to create a calibration plot relating electrophoretic mobility to molecular mass. The calculated weight-average molecular mass was 1900 kDa, closely similar to the reported 1700 kDa viscosity-average molecular mass of the sample. The peak in the densitometric curve corresponded to a molecular mass of about 2100 kDa.

For analysis of HA samples in the 5–500 kDa range, higher concentrations of agarose can be used in a Tris–borate–EDTA (TBE) buffer, where the borate slightly reduces the agarose gel network pore size and gives better pH stability during the run and improved compatibility with postelectrophoretic staining. Alternatively, polyacrylamide gels in TBE with a gradient in polyacrylamide concentration from 4% to 20% are widely used and available commercially as precast gels. Sample loads are usually 0.5–1.0 μg for polyacrylamide gels, and 1.0–2.5 μg for agarose gels. Fig. 18 shows the polyacrylamide gel electrophoresis (PAGE) result for the

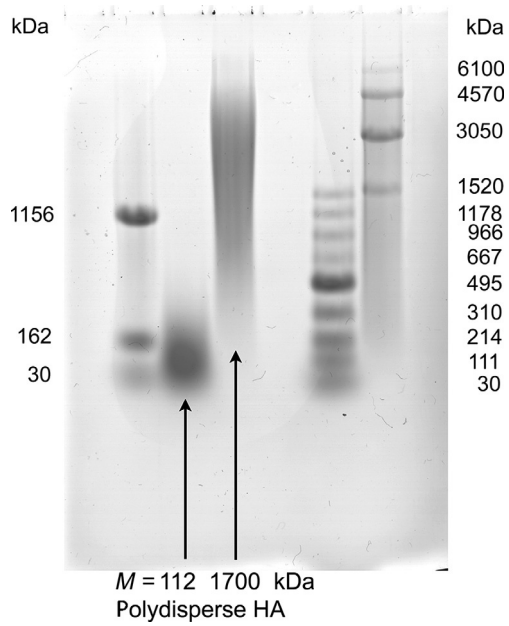

Fig. 16 The molecular mass distribution of high-molecular-mass HA was analyzed by electrophoresis on a 0.5% agarose gel with detection by Stains-All dye. Low polydispersity HA standards (Select-HA) created by chemoenzymatic synthesis appeared as discrete bands, but HA isolated from tissue or bacterial sources appeared highly polydisperse. The viscosity-average molecular mass of the two polydisperse samples is indicated. *This figure has been adapted with permission from Cowman, M. K.; Chen, C. C.; Pandya, M.; Yuan, H.; Ramkishun, D.; LoBello, J.; Bhilocha, S.; Russell-Puleri, S.; Skendaj, E.; Mijovic, J.; Jing, W. Improved Agarose Gel Electrophoresis Method and Molecular Mass Calculation for High Molecular Mass Hyaluronan.* Anal. Biochem. ***2011,*** 417, *50–56. Copyright 2011, Elsevier Inc.*

analysis of several commercially available, polydisperse, pure HA samples with low-average molecular mass. The viscosity-average molecular mass of each sample is indicated in the figure.

The best choice of gel type and concentration depends on the range of sizes in an HA sample. Fig. 19 shows densitometric scans of four polydisperse samples calibrated to molecular mass by coelectrophoresis of nearly monodisperse HA standards. A 3% agarose gel in TBE buffer was used for the 112 and 59 kDa samples. A 4% agarose gel in TBE was used for the 37 kDa HA sample. For the 22 kDa HA, a 4%–20% polyacrylamide gel

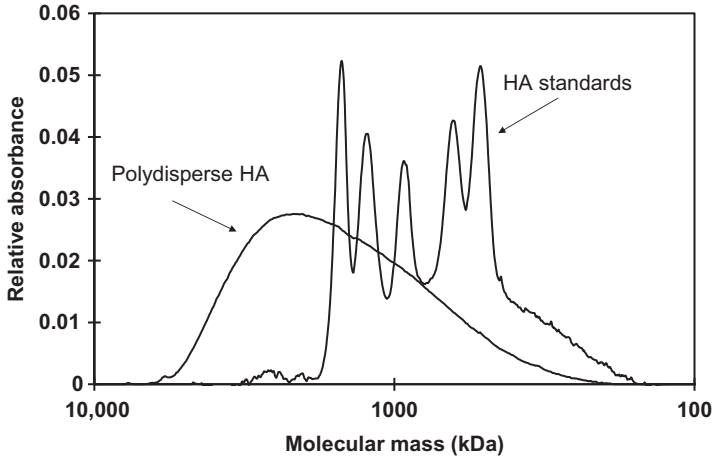

Fig. 17 Quantification of HA molecular mass distribution was achieved by densitometric analysis of a stained agarose gel following electrophoresis. The densitometric data for an unknown sample were calibrated using coelectrophoresis of low polydispersity HA standards of known size to convert migration distance to HA molecular mass. *This figure has been reproduced with permission from Cowman, M. K.; Chen, C. C.; Pandya, M.; Yuan, H.; Ramkishun, D.; LoBello, J.; Bhilocha, S.; Russell-Puleri, S.; Skendaj, E.; Mijovic, J.; Jing, W. Improved Agarose Gel Electrophoresis Method and Molecular Mass Calculation for High Molecular Mass Hyaluronan.* Anal. Biochem. ***2011,*** 417, *50–56. Copyright 2011, Elsevier Inc.*

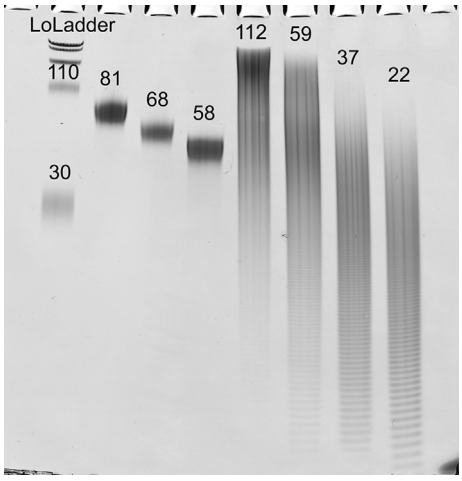

Fig. 18 The molecular mass distribution of low-molecular-mass HA was analyzed by electrophoresis on a 4%–20% gradient polyacrylamide gel with detection by Stains-All dye. Low polydispersity HA standards (Select-HA) created by chemoenzymatic synthesis appeared as discrete bands. HA samples obtained by controlled degradation of high-molecular-mass bacterial HA appeared highly polydisperse. The viscosity-average molecular masses of the polydisperse samples are indicated. *This figure has been adapted with permission from Bhilocha, S.; Amin, R.; Pandya, M.; Yuan, H.; Tank, M.; LoBello, J.; Shytuhina, A.; Wang, W.; Wisniewski, H. G.; de la Motte, C.; Cowman, M. K. Agarose and Polyacrylamide Gel Electrophoresis Methods for Molecular Mass Analysis of 5- to 500-kDa Hyaluronan.* Anal. Biochem. ***2011,*** 417, *41–49. Copyright 2011, Elsevier Inc.*

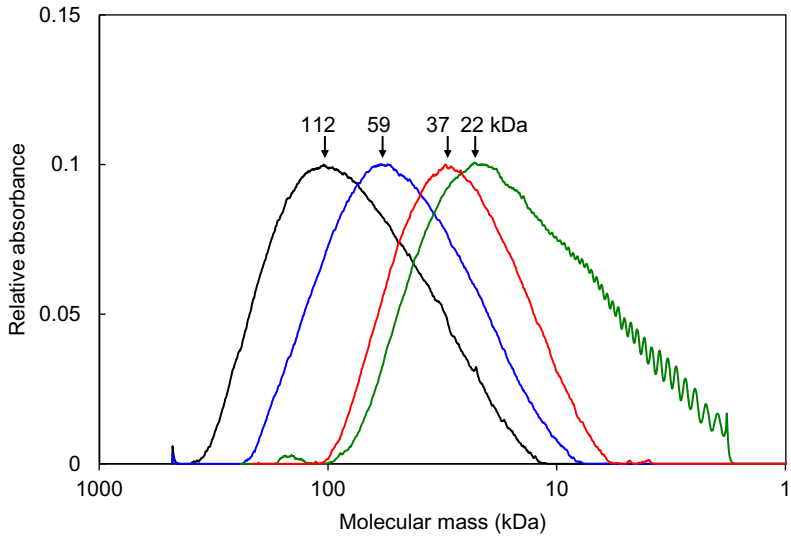

Fig. 19 The best electrophoretic gel choice depends on the molecular mass range present in an HA sample. Densitometric profiles presented for several polydisperse HA samples with low-average molecular mass are labeled with the viscosity-average molecular mass for each sample indicated above the corresponding profile. The gel types used were as follows: 3% agarose for 112- and 59-kDa HA, 4% agarose for 37-kDa HA, and 4%–20% polyacrylamide for 22-kDa HA. Absorbance data were scaled to the same maximum height in each profile for facile comparison. *This figure has been adapted with permission from Bhilocha, S.; Amin, R.; Pandya, M.; Yuan, H.; Tank, M.; LoBello, J.; Shytuhina, A.; Wang, W.; Wisniewski, H. G.; de la Motte, C.; Cowman, M. K. Agarose and Polyacrylamide Gel Electrophoresis Methods for Molecular Mass Analysis of 5- to 500-kDa Hyaluronan.* Anal. Biochem. ***2011,*** 417, *41–49. Copyright 2011, Elsevier Inc.*

in TBE was used. The gel composition choice was made to ensure that all of the HA in a given sample was within the linear calibration range for the gel used.

It is not always possible to use nonspecific staining of electrophoretic gels to determine HA molecular mass distribution. Contaminants that migrate similarly to HA and that bind cationic dyes can be present. As an alternative approach, a combination of ion-exchange chromatography (IEX) for fractionation and ELISA-like assay for quantification can be used.[125] Although IEX is most commonly employed to separate sulfated glycosaminoglycans from nonsulfated HA or chondroitin, it is possible to fractionate HA by size over a size range from oligosaccharides to approximately 100 kDa, as the

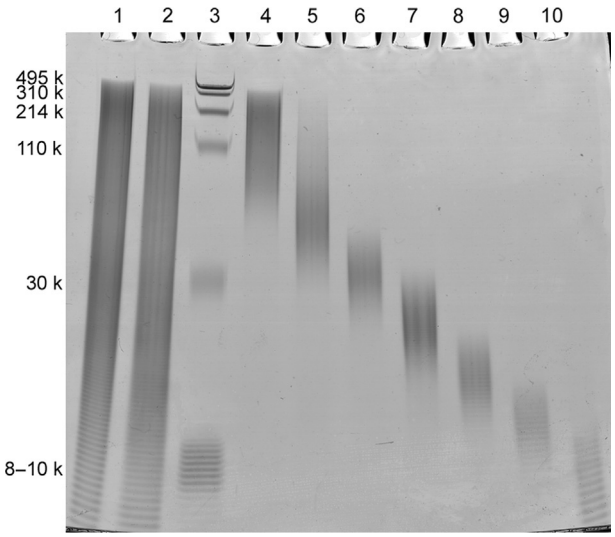

Fig. 20 Fractionation of HA by ion-exchange chromatography. A polydisperse HA sample was fractionated by stepwise elution from an anion-exchange spin column using seven NaCl solutions of increasing concentrations, then analyzed by electrophoresis on a 4%–20% gradient polyacrylamide gel. Lane 1: untreated polydisperse HA, 4 μg; lane 2: mixture of equal portions of the isolated IEX fractions (recombined), 4 μg if no loss occurred; lane 3: Select-HA molecular mass markers of 495, 310, 214, 110, and 30 kDa in addition to purified 7.6- to 10-kDa HA; lanes 4–10: HA eluted with 0.800, 0.440, 0.416, 0.400, 0.360, 0.330, and 0.300 M NaCl solutions, respectively. *This figure has been reproduced with permission from Yuan, H.; Amin, R.; Ye, X.; de la Motte, C. A.; Cowman, M. K. Determination of Hyaluronan Molecular Mass Distribution in Human Breast Milk.* Anal. Biochem. ***2015,*** *474, 78–88. Copyright 2015, Elsevier Inc.*

affinity of anionic HA for the cationic resin is dependent on total charge. Longer chains require elution with salt solutions of increasing ionic strength. A step gradient of NaCl from 0.30 to 0.80 M NaCl can be used to elute HA fractions of increasing molecular mass. Fig. 20 shows the PAGE analysis of HA fractions obtained by step gradient elution from a spin IEX column. A set of seven low polydispersity fractions were obtained. Coupling the IEX fractionation with a sensitive ELISA-like assay (Fig. 21) allows specific determination of HA and is suitable for detecting the presence of low-molecular-mass HA in biological samples containing total HA at low concentration.

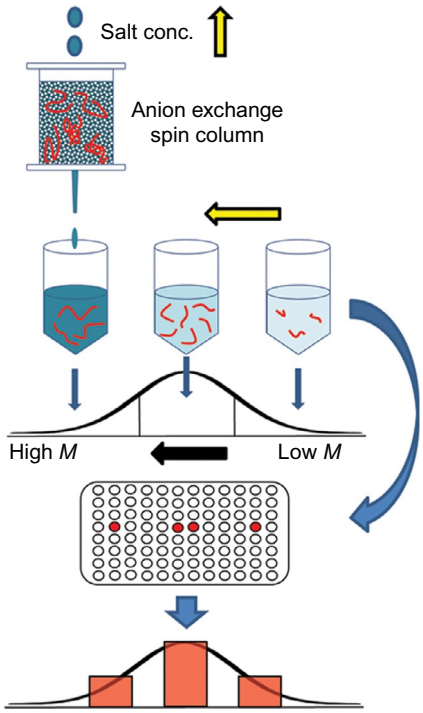

Fig. 21 Scheme for determination of HA molecular mass distribution by ion-exchange fractionation and specific HA quantification. HA was fractionated according to molecular mass using stepwise elution from an anion-exchange column with solutions of increasing salt concentrations. HA in each fraction was quantified by competitive ELISA-like assay. *This figure has been reproduced with permission from Yuan, H.; Amin, R.; Ye, X.; de la Motte, C. A.; Cowman, M. K. Determination of Hyaluronan Molecular Mass Distribution in Human Breast Milk.* Anal. Biochem. ***2015,*** *474, 78–88. Copyright 2015, Elsevier Inc.*

6.4 Experimental Findings on HA Content and Size

There are multiple studies correlating changes in HA content and size with tissue remodeling and inflammatory pathological processes.

6.4.1 HA in Biological Fluids

The concentration of HA in biological fluids can sometimes be determined without purification using specific detection as by ELISA-like assay. If the HA is bound to proteins such as aggrecan or versican, it will be incompletely detected unless the bound protein is enzymatically digested prior to assay. HA in synovial fluid, blood serum, and milk has low levels of bound protein,

but HA in conditioned medium from cultured cells can have significant bound protein and must be treated with a protease prior to assay. For the most accurate determination of HA molecular mass, it is usually preferred to remove protein, lipid, and small-molecule contaminants prior to analysis by chromatographic or electrophoretic methods.

Normal human knee joint synovial fluid contains HA at a concentration of about 2–3 mg/mL.[13,15] In osteoarthritis (OA) or rheumatoid arthritis (RA), the concentration can be reduced, especially in the presence of effusion that increases synovial fluid volume.[13,267,272] The average molecular mass of the HA in normal humans is near 6000–7000 kDa,[13,267,270] but can be significantly reduced in OA or RA due to inflammation. Fig. 22 shows the molecular mass distribution of HA in normal and OA patient synovial fluids as determined by agarose gel electrophoresis.[6,270] The OA patient fluids were highly variable in the extent of HA molecular mass reduction. The combination of the HA concentration and molecular mass in synovial fluid places this fluid in the semidilute solution regime where viscosity depends on $c[\eta]$ to the 3rd to 4th power due to macromolecular crowding. The loss of viscosity can then be substantial. For the OA synovial fluids, modest reductions in average molecular mass (e.g., from 6000 to 4000 kDa, corresponding to an intrinsic viscosity decrease from 7700 to 5500 mL/g) and concentration (e.g., from 2.5 to 1.5 mg/mL) would cause a significant drop in the coil overlap parameter (from ca. 19 to 8), leading to a nearly 18-fold drop (from ca. 2100 to 120) in specific viscosity of synovial fluid.

The normal HA concentration in human serum is usually less than about 40 ng/mL. It is elevated in hepatic cirrhosis,[273] in rheumatoid arthritis,[260,274] in ankylosing spondylitis,[260] and in osteoarthritis.[255,260] Untreated cancer is associated with an increase in serum HA.[253,275–277] The size of the HA in normal and RA blood serum is low to moderate, averaging about 100–500 kDa.[269,274,277] The presence of (undefined) low-molecular-mass HA in serum of cancer patients has been suggested to be useful in differentiating metastatic from nonmetastatic breast cancer.[278] In contrast, patients with Wilms' renal tumors had high levels of high-molecular-mass HA (ca. 2000 kDa).[277]

Normal human urine contains HA at a concentration of about 100–300 ng/mL,[231] and it is mainly low to moderate in molecular mass, although bladder cancer patients also showed the presence of high-molecular-mass HA.[279]

Human milk has a low concentration of HA, decreasing from about 800 ng/mL in the first week after birth to about 200 ng/mL at >60 days

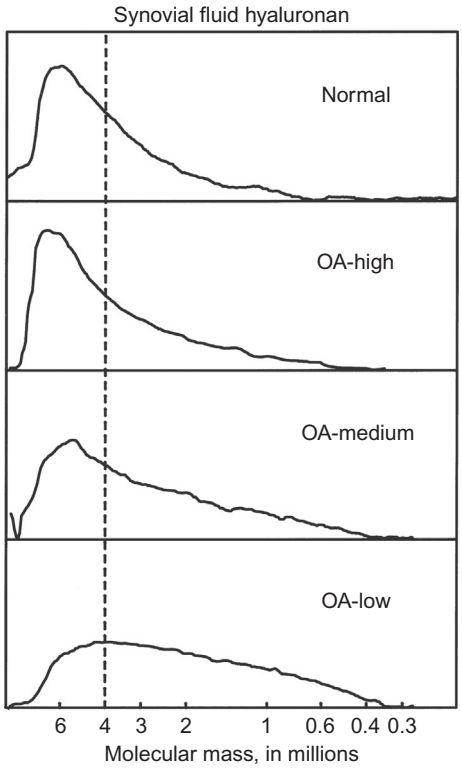

Fig. 22 Electrophoretic analysis of the molecular mass distribution of HA in human synovial fluid (SF) from normal and osteoarthritic (OA) patients. Normal: human SF obtained from young healthy volunteers; OA-high/medium/low: osteoarthritis patient SF patterns representative of three classes of samples. The percentage of HA with *M* greater than 4 MDa was 61% (normal), 61% (OA-high), 45% (OA-medium), and 27% (OA-low). In analysis of 39 OA patient SF, the average fraction of HA >4 MDa was 48 ± 15%, similar to the OA-medium-type sample. *This figure has been reproduced with permission from Cowman, M. K.; Lee, H. G.; Schwertfeger, K. L.; McCarthy, J. B.; Turley, E. A. The Content and Size of Hyaluronan in Biological Fluids and Tissues.* Front. Immunol. ***2015,*** *6, 261. Copyright 2015, the authors.*

postpartum.[24] The HA component of milk contributes to defense of the infant's intestinal epithelium against microbial infection via interaction with CD44 and TLR4 receptors, resulting in the expression of the antimicrobial peptide human β-defensin 2.[24] The size distribution of the HA is critical to this effect. About 95% of milk HA is moderate in molecular mass, averaging about 440 kDa, based on agarose gel electrophoretic analysis (Fig. 23).[125] This size of HA can provide multivalent binding to clustered CD44 at

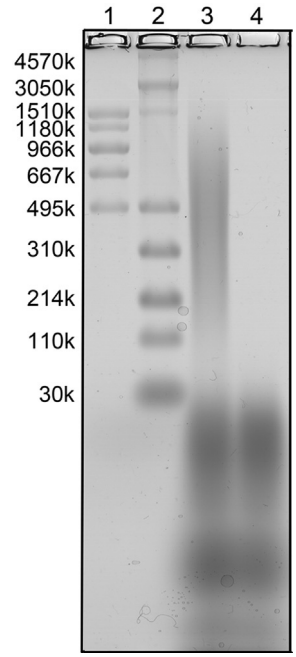

Fig. 23 Molecular mass distribution for human milk HA by 1% agarose gel electrophoresis. Lanes 1 and 2: Select-HA standards. Lane 3: approximately 2.5 μg of HA, obtained as the highest-molecular-mass fraction of milk HA after elution from an IEX column; lane 4: the same sample as in lane 3 but after specific hyaluronidase digestion. The bands migrating faster than the 100-kDa HA standard are impurities and do not contain any HA. *This figure has been reproduced with permission from Yuan, H.; Amin, R.; Ye, X.; de la Motte, C. A.; Cowman, M. K. Determination of Hyaluronan Molecular Mass Distribution in Human Breast Milk.* Anal. Biochem. ***2015,*** 474*, 78–88. Copyright 2015, Elsevier Inc.*

the cell surface. It is more difficult to analyze for the presence of bioactive lower-molecular-mass HA in milk without complete purification. Using biotinylated HABP to bind HA and magnetic beads bearing streptavidin to pull down the complex, a very low level of HA with a molecular mass of about 35 kDa was discovered (Fig. 24).[125] In analysis of milk from 20 unique donors using the IEX–ELISA method, the presence of the low-molecular-mass HA was confirmed (Fig. 25). The HA fragments can act as danger-associated molecular patterns, critical to both the stimulation of TLR4 receptors and the antimicrobial peptide production so important for infant health.

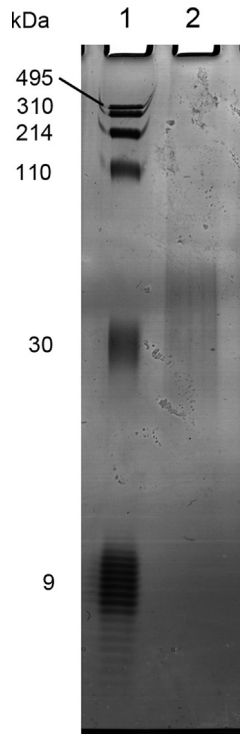

Fig. 24 Low-*M* HA isolated from human milk was analyzed by 4%–20% polyacrylamide gel electrophoresis. Lane 1: LoLadder containing HA molecular mass markers 495, 310, 214, 110, and 30 kDa in addition to purified 7.6- to 10.0-kDa (average ca. 9.0 kDa) HA; lane 2: milk HA from a 0.425 M NaCl elution from IEX captured by specific binding to bVG1 and streptavidin-coated magnetic beads. *This figure has been reproduced with permission from Yuan, H.; Amin, R.; Ye, X.; de la Motte, C. A.; Cowman, M. K. Determination of Hyaluronan Molecular Mass Distribution in Human Breast Milk.* Anal. Biochem. ***2015,*** *474, 78–88. Copyright 2015, Elsevier Inc.*

6.4.2 HA in Tissues

The tissue with the highest HA content is cartilage. Human articular cartilage contains about 500–2500 μg HA per g wet tissue.[233] The HA serves to organize the aggrecan proteoglycans of the extracellular matrix, resulting in a highly hydrated supporting network responsible for the compression resistance properties of cartilage. The HA is synthesized as a high-molecular-mass polymer averaging about 2000 kDa, but is found in a partially degraded 300 kDa form in older persons.[233]

Human skin also has a high content of HA (averaging about 400–500 μg/g wet tissue), and it is present at higher levels in fetal and young

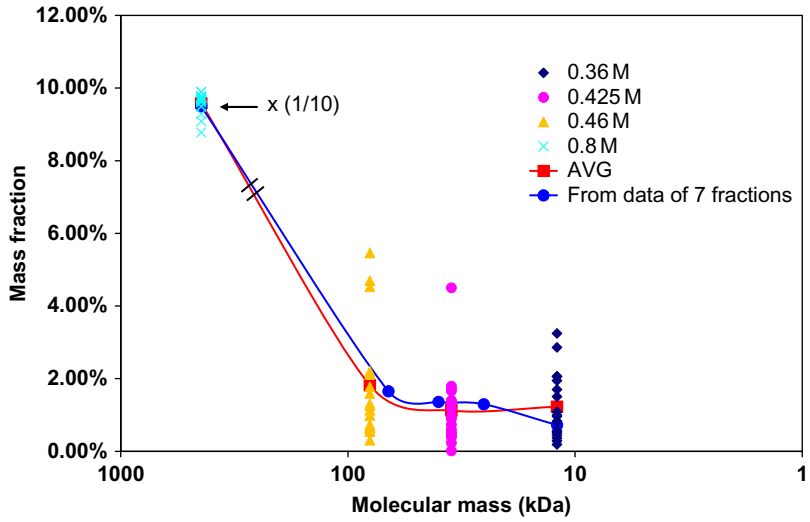

Fig. 25 Human milk HA has a detectable fraction of low-molecular-mass bioactive HA. The HA size distribution for 20 human milk HA samples was determined by IEX fractionation and content analysis by competitive ELISA-like assay. *This figure has been reproduced with permission from Yuan, H.; Amin, R.; Ye, X.; de la Motte, C. A.; Cowman, M. K. Determination of Hyaluronan Molecular Mass Distribution in Human Breast Milk.* Anal. Biochem. ***2015,*** *474, 78–88. Copyright 2015, Elsevier Inc.*

skin in comparison with older skin.[280] The HA has very high molecular mass, averaging 4000–6000 kDa. Following irradiation with UVB, HA size is reduced.[281] Rat skin similarly has high-molecular-mass HA (>3000 kDa).[126]

Other healthy organs have lower HA contents. Laurent and Tengblad[231] found HA generally present at 1–100 μg/g wet tissue in rabbit cornea, liver, muscle, brain, and kidney. Similarly, Armstrong and Bell[163] found HA content to be approximately 100–200 μg/g tissue in rabbit lung, muscle, small intestine, large intestine, and heart. In all healthy tissues, the HA size was high in molecular mass, averaging about 4000–6000 kDa.

High levels of HA are found in carcinomas of the lung, colorectal, prostate, bladder, and breast tissues. The increase in HA level is linked to tumor aggression.[232,234,235,282,283] Other tissues undergoing rapid remodeling also have elevated HA content. Mammary gland morphogenesis is accompanied by changes in HA content, with the highest levels found associated with gland remodeling during gestation.[284] Healing of rat or mouse skin wounds is associated with an approximately twofold increase in HA content and the presence of fragmented HA (Fig. 26).[126,236]

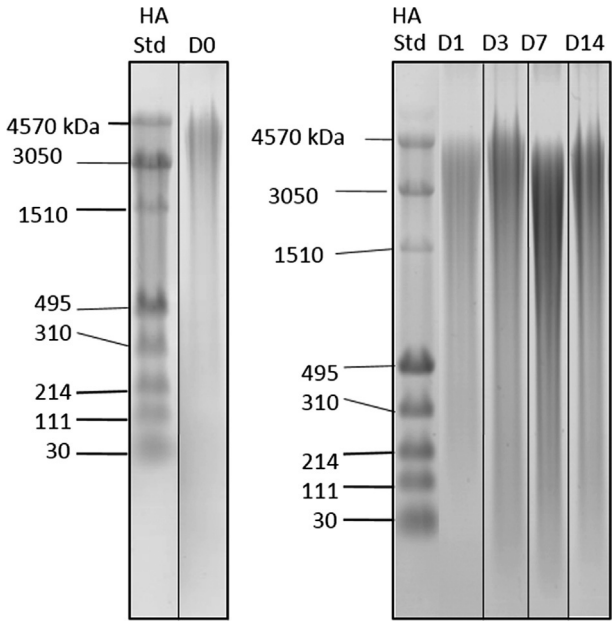

Fig. 26 Low-molecular-mass HA appears during healing of wounds. Agarose gel electrophoretic analysis of HA isolated from full-thickness excisional rat skin wounds 0–14 days (D) after wounding. HA was visualized in the electrophoretic gels by Stains-All dye. Mainly high-molecular-mass HA was present at day 0, but a broad distribution of HA sizes appeared by day 3 and was prominently observed at day 7. *This figure has been adapted from Tolg, C.; Hamilton, S. R.; Zalinska, E.; McCulloch, L.; Amin, R.; Akentieva, N.; Winnik, F.; Savani, R.; Bagli, D. J.; Luyt, L. G.; Cowman, M. K.; McCarthy, J. B.; Turley, E. A. A RHAMM Mimetic Peptide Blocks Hyaluronan Signaling and Reduces Inflammation and Fibrogenesis in Excisional Skin Wounds.* Am. J. Pathol. ***2012,*** 181, *1250–1270. Copyright 2012, American Society for Investigative Pathology.*

7. DIAGNOSTIC AND THERAPEUTIC APPLICATIONS

Fig. 27 illustrates the concept behind much of our work. Knowledge gained by the study of HA in biological environments can be exploited to develop new diagnostic and therapeutic approaches to combat disease.

7.1 Exogenous HA

Semidilute solutions of pure high-molecular-mass HA are widely used as viscoelastic tools in ophthalmic surgery,[26] and as intraarticularly injected analgesic treatments for osteoarthritis.[25,285] These medical applications rely principally on the mechanical properties of HA solutions. Coupling our

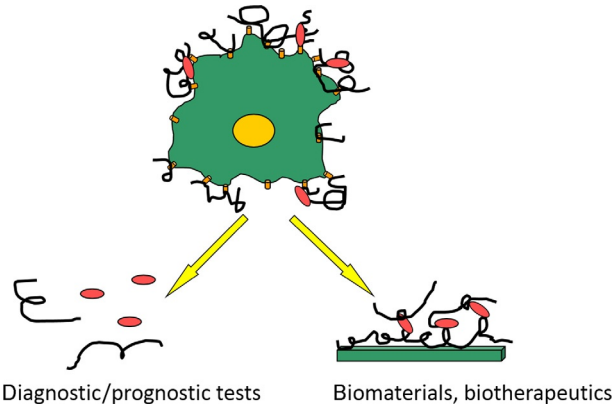

Fig. 27 Improved understanding of HA structure and function in vivo is leading to new diagnostic and therapeutic applications.

understanding of the worm-like coil conformation for high-molecular-mass HA in neutral aqueous salt solutions and the effects of coil overlap that cause nonideality even at low concentrations, it is possible to control the medically important physicochemical properties (viscoelastic cushioning, lubrication) of therapeutic HA solutions by varying the HA concentration and molecular mass. For example, the Matsuoka–Cowman theory for mutual macromolecular crowding shows that increasing the elastic modulus requires only a change in HA concentration, but increasing viscosity can be accomplished by increasing either or both HA concentration and molecular mass.

The recognition that HA-based treatments have effects that outlast the residence time of HA in the tissue has turned attention to control of the biological signaling properties of HA.[10] Through its interaction with CD44, exogenous high-molecular-mass HA can counteract the proinflammatory effects of IL-1β and TNF-α in chondrocytes and synoviocytes.[286] Orally administered high-molecular-mass HA can enhance the production of the antiinflammatory cytokine IL-10 via TLR4 on intestinal epithelial cells.[287] If HA is modified by the TSG-6-catalyzed covalent attachment of heavy chains from IαI, the resulting cross-linked matrix creates a microenvironment that supports stem cells in tissue repair by an as-yet-unknown mechanism.[288,289]

Exogenous low-molecular-mass HA fragments have also been proposed for specific therapeutic applications. While generally regarded as proinflammatory, HA fragments are better viewed as prodefensive in specific environments. HA tetrasaccharides are reported to suppress the expression

of IL-1β by hippocampal neurons following hypoxic–ischemic brain injury via a TLR2-dependent mechanism.[290] HA hexasaccharides are reported to stimulate fibroblast migration and improve wound closure by a mechanism involving both CD44 and RHAMM proteins.[291] Orally ingested HA fragments of about 35 kDa are able to induce the expression of the antimicrobial peptide β-defensin 2 in the intestinal epithelium of mice via a TLR4-dependent mechanism.[23] In human milk containing moderate-molecular-mass HA of about 440 kDa and low-molecular-mass HA of 35 kDa, both TLR4 and CD44 are stimulated to upregulate human β-defensin 2 in cultured colonic epithelial cells.[24,125]

These recent developments in our understanding of the antiinflammatory cell-signaling effects of HA suggest that there will be continuing interest in HA-based therapeutics.

7.2 HA-Based Medical Diagnostics

In serum, the content of HA is increased in several diseases, particularly if there is an inflammatory component to the pathology. Because the liver is responsible for HA uptake from the blood, a high HA level in serum is part of a multicomponent diagnostic for hepatic cirrhosis.[273,292,293] Liver fibrosis, severe fibrosis, and cirrhosis can be discriminated by different serum HA level cutoffs.

Tumor tissues produce high levels of HA, and cancers can cause blood serum HA levels to be elevated.[253,275,294] Interestingly, it was found that the content of low-molecular-mass HA in serum can be used to differentiate metastatic from nonmetastatic breast cancer.[278]

Urinary HA is a specific biomarker for bladder cancer.[279,295]

We recently found that mouse mammary primary tumors, as well as lung metastases, had high levels of degraded HA (Tolg, Yuan, Cowman, and Turley, unpublished). This suggests the possibility that analysis of the size distribution of HA in tumor tissues may be useful in predicting tumor progression or in stratifying patients for treatment decisions.[21]

7.3 Therapeutic Modulation of HA Signaling

There is great interest in the development of therapeutics to modulate proinflammatory signaling by HA fragments. One approach is to use antioxidants to reduce the levels of ROS/RNS in order to reduce the production of HA fragments. A second approach is to develop molecular tools to block the signaling by HA fragments. Turley and coworkers have identified

HA-binding peptides that have homology to the HA receptor protein RHAMM.[126] A 15-mer peptide that disrupts HA binding to RHAMM was found to promote healing of excisional skin wounds in the rat, without fibrosis. The same peptide, formulated with high-molecular-mass HA, has shown promise for regenerative healing of cartilage by control of inflammation and stem-cell differentiation (Cowman, Kirsch, Strauss, Turley, Toelg, Luyt, PCT/US2015/045934). The mixture of high-molecular-mass HA and an HA-binding peptide acts synergistically to favor healing without fibrosis. These studies suggest that control of cell signaling by HA and HA fragments may hold the key to regenerative repair of many types of tissues and to the modulation of inflammatory disease processes in which HA plays a role.

ACKNOWLEDGMENTS

The author wishes to thank her many collaborators for their insights and support. Special thanks are due to Dr. Endre A. Balazs, Dr. Shiro Matsuoka, Dr. Carol de la Motte, Dr. Eva Turley, and Dr. Thorsten Kirsch, and to the graduate students who contributed so much, including Dr. Hoki Min, Dr. Hong Gee Lee, Dr. Dina Kudasheva, Dr. Chiara Spagnoli, Dr. Han Yuan, Ripal Amin, Shardul Bhilocha, and Monika Pandya, among many others. The author also thanks undergraduate student Gyu Ik Jung for preparation of Fig. 1.

REFERENCES

1. Weissmann, B.; Meyer, K.; Sampson, P.; Linker, A. Isolation of Oligosaccharides Enzymatically Produced From Hyaluronic Acid. *J. Biol. Chem.* **1954**, *208*, 417–429.
2. Min, H.; Cowman, M. K. Combined Alcian Blue and Silver Staining of Glycosaminoglycans in Polyacrylamide Gels: Application to Electrophoretic Analysis of Molecular Weight Distribution. *Anal. Biochem.* **1986**, *155*, 275–285.
3. Itano, N. Simple Primary Structure, Complex Turnover Regulation and Multiple Roles of Hyaluronan. *J. Biochem.* **2008**, *144*, 131–137.
4. Vigetti, D.; Karousou, E.; Viola, M.; Deleonibus, S.; De Luca, G.; Passi, A. Hyaluronan: Biosynthesis and Signaling. *Biochim. Biophys. Acta* **2014**, *1840*, 2452–2459.
5. Tammi, R. H.; Passi, A. G.; Rilla, K.; Karousou, E.; Vigetti, D.; Makkonen, K.; Tammi, M. I. Transcriptional and Post-translational Regulation of Hyaluronan Synthesis. *FEBS J.* **2011**, *278*, 1419–1428.
6. Cowman, M. K.; Lee, H. G.; Schwertfeger, K. L.; McCarthy, J. B.; Turley, E. A. The Content and Size of Hyaluronan in Biological Fluids and Tissues. *Front. Immunol.* **2015**, *6*, 261.
7. Cowman, M. K.; Matsuoka, S. Experimental Approaches to Hyaluronan Structure. *Carbohydr. Res.* **2005**, *340*, 791–809.
8. Petrey, A. C.; de la Motte, C. A. Hyaluronan, a Crucial Regulator of Inflammation. *Front. Immunol.* **2014**, *5*, 101.
9. Cyphert, J. M.; Trempus, C. S.; Garantziotis, S. Size Matters: Molecular Weight Specificity of Hyaluronan Effects in Cell Biology. *Int. J. Cell Biol.* **2015**, *2015, 563818.*
10. Liang, J.; Jiang, D.; Noble, P. W. Hyaluronan as a Therapeutic Target in Human Diseases. *Adv. Drug Deliv. Rev.* **2016**, *97*, 186–203.

11. Fraser, J. R.; Laurent, T. C.; Laurent, U. B. Hyaluronan: Its Nature, Distribution, Functions and Turnover. *J. Intern. Med.* **1997**, *242*, 27–33.
12. Laurent, T. C.; Laurent, U. B.; Fraser, J. R. The Structure and Function of Hyaluronan: An Overview. *Immunol. Cell Biol.* **1996**, *74*, A1–7.
13. Balazs, E. A. Viscoelastic Properties of Hyaluronic Acid and Biological Lubrication. *Univ. Mich. Med. Cent. J.* **1968**, 255–259.
14. Cowman, M. K.; Schmidt, T. A.; Raghavan, P.; Stecco, A. Viscoelastic Properties of Hyaluronan in Physiological Conditions. *F1000Res* **2015**, *4*, 622.
15. Balazs, E. A.; Watson, D.; Duff, I. F.; Roseman, S. Hyaluronic Acid in Synovial Fluid. I. Molecular Parameters of Hyaluronic Acid in Normal and Arthritis Human Fluids. *Arthritis Rheum.* **1967**, *10*, 357–376.
16. Balazs, E. A. Fine Structure and Function of Ocular Tissues. The Vitreous. *Int. Ophthalmol. Clin.* **1973**, *13*, 169–187.
17. Hardingham, T. E.; Fosang, A. J. Proteoglycans: Many Forms and Many Functions. *FASEB J.* **1992**, *6*, 861–870.
18. Evanko, S. P.; Tammi, M. I.; Tammi, R. H.; Wight, T. N. Hyaluronan-Dependent Pericellular Matrix. *Adv. Drug Deliv. Rev.* **2007**, *59*, 1351–1365.
19. Laurent, T. C. The Interaction Between Polysaccharides and Other Macromolecules. 9. The Exclusion of Molecules From Hyaluronic Acid Gels and Solutions. *Biochem. J.* **1964**, *93*, 106–112.
20. Laurent, T. C. An Early Look at Macromolecular Crowding. *Biophys. Chem.* **1995**, *57*, 7–14.
21. Schwertfeger, K. L.; Cowman, M. K.; Telmer, P. G.; Turley, E. A.; McCarthy, J. B. Hyaluronan, Inflammation, and Breast Cancer Progression. *Front. Immunol.* **2015**, *6*, 236.
22. Jiang, D.; Liang, J.; Noble, P. W. Hyaluronan as an Immune Regulator in Human Diseases. *Physiol. Rev.* **2011**, *91*, 221–264.
23. Hill, D. R.; Kessler, S. P.; Rho, H. K.; Cowman, M. K.; de la Motte, C. A. Specific-Sized Hyaluronan Fragments Promote Expression of Human Beta-Defensin 2 in Intestinal Epithelium. *J. Biol. Chem.* **2012**, *287*, 30610–30624.
24. Hill, D. R.; Rho, H. K.; Kessler, S. P.; Amin, R.; Homer, C. R.; McDonald, C.; Cowman, M. K.; de la Motte, C. A. Human Milk Hyaluronan Enhances Innate Defense of the Intestinal Epithelium. *J. Biol. Chem.* **2013**, *288*, 29090–29104.
25. Balazs, E. A.; Band, P. A. Therapeutic Use of Hyaluronan-Based Products. In: *Carbohydrate Chemistry, Biology and Medical Applications*; Garg, H. G., Cowman, M. K., Hales, C. A., Eds.; Elsevier: Amsterdam, 2008 pp 311–332.
26. Balazs, E. A. Hyaluronan as an Ophthalmic Viscoelastic Device. *Curr. Pharm. Biotechnol.* **2008**, *9*, 236–238.
27. Balazs, E. A. Analgesic Effect of Elastoviscous Hyaluronan Solutions and the Treatment of Arthritic Pain. *Cells Tissues Organs* **2003**, *174*, 49–62.
28. Guss, J. M.; Hukins, D. W. L.; Smith, P. J. C.; Winter, W. T.; Arnott, S.; Moorhouse, R.; Rees, D. A. Hyaluronic Acid: Molecular Conformations and Interactions in Two Sodium Salts. *J. Mol. Biol.* **1975**, *95*, 359–384.
29. Winter, W. T.; Smith, P. J. C.; Arnott, S. Hyaluronic Acid: Structure of a Fully Extended 3-Fold Helical Sodium Salt and Comparison With the Less Extended 4-Fold Helical Forms. *J. Mol. Biol.* **1975**, *99*, 219–235.
30. Winter, W. T.; Arnott, S. Hyaluronic Acid: The Role of Divalent Cations in Conformation and Packing. *J. Mol. Biol.* **1977**, *117*, 761–784.
31. Sheehan, J. K.; Atkins, E. D. T. X-Ray Fibre Diffraction Study of Conformational Changes in Hyaluronate Induced in the Presence of Sodium, Potassium and Calcium Cations. *Int. J. Biol. Macromol.* **1983**, *5*, 215–221.

32. Sheehan, J. K.; Gardner, K. H.; Atkins, E. D. T. Hyaluronic Acid: A Double-Helical Structure in the Presence of Potassium at Low pH and Found Also With the Cations Ammonium, Rubidium and Caesium. *J. Mol. Biol.* **1977**, *117*, 113–135.
33. Arnott, S.; Mitra, A. K.; Raghunathan, S. Hyaluronic Acid Double Helix. *J. Mol. Biol.* **1983**, *169*, 861–872.
34. Morgelin, M.; Paulsson, M.; Hardingham, T. E.; Heinegard, D.; Engel, J. Cartilage Proteoglycans. Assembly With Hyaluronate and Link Protein as Studied by Electron Microscopy. *Biochem. J.* **1988**, *253*, 175–185.
35. Scott, J. E.; Cummings, C.; Brass, A.; Chen, Y. Secondary and Tertiary Structures of Hyaluronan in Aqueous Solution, Investigated by Rotary Shadowing-Electron Microscopy and Computer Simulation. Hyaluronan Is a Very Efficient Network-Forming Polymer. *Biochem. J.* **1991**, *274*(Pt. 3), 699–705.
36. Scott, J. E.; Thomlinson, A. M.; Prehm, P. Supramolecular Organization in Streptococcal Pericellular Capsules Is Based on Hyaluronan Tertiary Structures. *Exp. Cell Res.* **2003**, *285*, 1–8.
37. Mikelsaar, R. H.; Scott, J. E. Molecular Modelling of Secondary and Tertiary Structures of Hyaluronan, Compared With Electron Microscopy and NMR Data. Possible Sheets and Tubular Structures in Aqueous Solution. *Glycoconjugate J.* **1994**, *11*, 65–71.
38. Cowman, M. K.; Li, M.; Balazs, E. A. Tapping Mode Atomic Force Microscopy of Hyaluronan: Extended and Intramolecularly Interacting Chains. *Biophys. J.* **1998**, *75*, 2030–2037.
39. Gunning, A. P.; Morris, V. J.; Al-Assaf, S.; Phillips, G. O. Atomic Force Microscopic Studies of Hylan and Hyaluronan. *Carbohydr. Polym.* **1996**, *30*, 1–8.
40. Cowman, M. K.; Li, M.; Dyal, A.; Balazs, E. A. Tapping Mode Atomic Force Microscopy of the Hyaluronan Derivative, Hylan A. *Carbohydr. Polym.* **2000**, *41*, 229–235.
41. Al-Assaf, S.; Phillips, G. O.; Gunning, A. P.; Morris, V. J. Molecular Interaction Studies of the Hyaluronan Derivative, Hylan A Using Atomic Force Microscopy. *Carbohydr. Polym.* **2002**, *47*, 341–345.
42. McIntire, T. M.; Brant, D. A. Imaging of Carrageenan Macrocycles and Amylose Using Noncontact Atomic Force Microscopy. *Int. J. Biol. Macromol.* **1999**, *26*, 303–310.
43. Spagnoli, C.; Loos, K.; Ulman, A.; Cowman, M. K. Imaging Structured Water and Bound Polysaccharide on Mica Surface at Ambient Temperature. *J. Am. Chem. Soc.* **2003**, *125*, 7124–7128.
44. Cowman, M. K.; Spagnoli, C.; Kudasheva, D.; Li, M.; Dyal, A.; Kanai, S.; Balazs, E. A. Extended, Relaxed, and Condensed Conformations of Hyaluronan Observed by Atomic Force Microscopy. *Biophys. J.* **2005**, *88*, 590–602.
45. Spagnoli, C.; Korniakov, A.; Ulman, A.; Balazs, E. A.; Lyubchenko, Y. L.; Cowman, M. K. Hyaluronan Conformations on Surfaces: Effect of Surface Charge and Hydrophobicity. *Carbohydr. Res.* **2005**, *340*, 929–941.
46. Cowman, M. K.; Spagnoli, C.; Kudasheva, D. S.; Matsuoka, S.; Balazs, E. A. Influence of Environment on Hyaluronan Shape. In: *Hyaluronan: Structure, Metabolism, Biological Activities, Therapeutic Applications*; Balazs, E. A., Hascall, V. C., Eds.; Vol. 1; Matrix Biology Institute: Edgewater, NJ, 2005; pp 79–87.
47. Laurent, T. C.; Ryan, M.; Pietruszkiewicz, A. Fractionation of Hyaluronic Acid. The Polydispersity of Hyaluronic Acid From the Bovine Vitreous Body. *Biochim. Biophys. Acta* **1960**, *42*, 476–485.
48. Fouissac, E.; Milas, M.; Rinaudo, M.; Borsali, R. Influence of the Ionic Strength on the Dimensions of Sodium Hyaluronate. *Macromolecules* **1992**, *25*, 5613–5617.
49. Takahashi, R.; Kubota, K.; Kawada, M.; Okamoto, A. Effect of Molecular Weight Distribution on the Solution Properties of Sodium Hyaluronate in 0.2M NaCl Solution. *Biopolymers* **1999**, *50*, 87–98.

50. Takahashi, R.; Al-Assaf, S.; Williams, P. A.; Kubnota, K.; Okamoto, A.; Nishinari, K. Asymmetrical-Flow Field-Flow Fractionation With On-line Multiangle Light Scattering Detection. 1. Application to Wormlike Chain Analysis of Weakly Stiff Polymer Chains. *Biomacromolecules* **2003**, *4*, 404–409.
51. Cowman, M. K.; Cozart, D.; Nakanishi, K.; Balazs, E. A. ^{1}H NMR of Glycosaminoglycans and Hyaluronic Acid Oligosaccharides in Aqueous Solution: The Amide Proton Environment. *Arch. Biochem. Biophys.* **1984**, *230*, 203–212.
52. Toffanin, R.; Kvam, B. J.; Flaibani, A.; Atzori, M.; Biviano, F.; Paoletti, S. NMR Studies of Oligosaccharides Derived From Hyaluronate: Complete Assignment of ^{1}H and ^{13}C NMR Spectra of Aqueous Di- and Tetra-Saccharides, and Comparison of Chemical Shifts for Oligosaccharides of Increasing Degree of Polymerisation. *Carbohydr. Res.* **1993**, *245*, 113–128.
53. Cowman, M. K.; Hittner, D. M.; Feder-Davis, J. ^{13}C-NMR Studies of Hyaluronan: Conformational Sensitivity to Varied Environments. *Macromolecules* **1996**, *29*, 2894–2902.
54. Cowman, M. K.; Feder-Davis, J.; Hittner, D. M. 13C NMR Studies of Hyaluronan. 2. Dependence of Conformational Dynamics on Chain Length and Solvent. *Macromolecules* **2001**, *34*, 110–115.
55. Balazs, E. A. Amino Sugar-Containing Macromolecules in the Tissues of the Eye and the Ear. In: *The Amino Sugars: The Chemistry and Biology of Compounds Containing Amino Sugars*; Balazs, E. A., Jeanloz, R. W., Eds.; Vol. 2A; Academic Press: New York, 1965; pp 401–460.
56. Shimada, E.; Matsumura, G. Viscosity and Molecular Weight of Hyaluronic Acids. *J. Biochem.* **1975**, *78*, 513–517.
57. Cleland, R. L. Viscometry and Sedimentation Equilibrium of Partially Hydrolyzed Hyaluronate: Comparison With Theoretical Models of Wormlike Chains. *Biopolymers* **1984**, *23*, 647–666.
58. Turner, R. E.; Lin, P. Y.; Cowman, M. K. Self-association of Hyaluronate Segments in Aqueous NaCl Solution. *Arch. Biochem. Biophys.* **1988**, *265*, 484–495.
59. Bothner, H.; Waaler, T.; Wik, O. Limiting Viscosity Number and Weight Average Molecular Weight of Hyaluronate Samples Produced by Heat Degradation. *Int. J. Biol. Macromol.* **1988**, *10*, 287–291.
60. Mendichi, R.; Šoltés, L.; Giacometti Schieroni, A. Evaluation of Radius of Gyration and Intrinsic Viscosity Molar Mass Dependence and Stiffness of Hyaluronan. *Biomacromolecules* **2003**, *4*, 1805–1810.
61. Hokputsa, S.; Jumel, K.; Alexander, C.; Harding, S. E. Hydrodynamic Characterisation of Chemically Degraded Hyaluronic Acid. *Carbohydr. Polym.* **2003**, *52*, 111–117.
62. Hayashi, K.; Tsutsumi, K.; Nakajima, F.; Norisuye, T.; Teramoto, A. Chain-Stiffness and Excluded-Volume Effects in Solutions of Sodium Hyaluronate at High Ionic Strength. *Macromolecules* **1995**, *28*, 3824–3830.
63. Hayashi, K.; Tsutsumi, K.; Norisuye, T.; Teramoto, A. Electrostatic Contributions to Chain Stiffness and Excluded-Volume Effects in Sodium Hyaluronate Solutions. *Polym. J.* **1996**, *28*, 922–928.
64. Cowman, M. K.; Matsuoka, S. The Intrinsic Viscosity of Hyaluronan. In: *Hyaluronan*; Kennedy, J. F., Phillips, G. O., Williams, P. A., Hascall, V. C., Eds.; Vol. 1; Woodhead Publishing Ltd.: Cambridge, 2002; pp 75–78
65. Ogston, A. G. The Spaces in a Uniform Random Suspension of Fibres. *Trans. Faraday Soc.* **1958**, *54*, 1754–1757.
66. Laurent, T. C.; Killander, J. A Theory of Gel Filtration and Its Exeperimental Verification. *J. Chromatogr. A* **1964**, *14*, 317–330.
67. Laurent, T. C. History of a Theory. *J. Chromatogr. A* **1993**, *633*, 1–8.

68. Kwei, T. K.; Nakazawa, M.; Matsuoka, S.; Cowman, M. K.; Okamoto, Y. Concentration Dependence of Solution Viscosities of Rigid Rod Polymers. *Macromolecules* **2000**, *33*, 235–236.
69. Matsuoka, S.; Cowman, M. K. Equation of State for Polymer Solution. *Polymer* **2002**, *43*, 3447–3453.
70. Cowman, M. K.; Hernandez, M.; Kim, J. R.; Yuan, H.; Hu, Y. Macromolecular Crowding in the Biomatrix. In: *Structure and Function of Biomatrix. Control of Cell Behavior and Gene Expression*; Balazs, E. A. Ed.; Matrix Biology Institute: Edgewater, NJ, 2012; pp 45–66.
71. Cowman, M. K. Mutual Macromolecular Crowding as the Basis for Polymer Solution Non-ideality. *Polym. Adv. Technol.* **2017**, *28*, 1000–1004.
72. Cowman, M. K.; Mendichi, R. Methods for Determination of Hyaluronan Molecular Weight. In: *Chemistry and Biology of Hyaluronan*; Garg, H. G., Hales, C. A., Eds.; Elsevier: Amsterdam, 2004; pp 41–69.
73. Cowman, M. K.; Chen, C. C.; Pandya, M.; Yuan, H.; Ramkishun, D.; LoBello, J.; Bhilocha, S.; Russell-Puleri, S.; Skendaj, E.; Mijovic, J.; Jing, W. Improved Agarose Gel Electrophoresis Method and Molecular Mass Calculation for High Molecular Mass Hyaluronan. *Anal. Biochem.* **2011**, *417*, 50–56.
74. Laurent, T. C.; Ogston, A. G. The Interaction Between Polysaccharides and Other Macromolecules. 4. The Osmotic Pressure of Mixtures of Serum Albumin and Hyaluronic Acid. *Biochem. J.* **1963**, *89*, 249–253.
75. Gibbs, D. A.; Merrill, E. W.; Smith, K. A.; Balazs, E. A. Rheology of Hyaluronic Acid. *Biopolymers* **1968**, *6*, 777–791.
76. Yanaki, T.; Yamaguchi, T. Temporary Network Formation of Hyaluronate Under a Physiological Condition. 1. Molecular-Weight Dependence. *Biopolymers* **1990**, *30*, 415–425.
77. Fouissac, E.; Milas, M.; Rinaudo, M. Shear-Rate, Concentration, Molecular Weight, and Temperature Viscosity Dependencies of Hyaluronate, a Wormlike Polyelectrolyte. *Macromolecules* **1993**, *26*, 6945–6951.
78. De Smedt, S. C.; Dekeyser, P.; Ribitsch, V.; Lauwers, A.; Demeester, J. Viscoelastic and Transient Network Properties of Hyaluronic Acid as a Function of the Concentration. *Biorheology* **1993**, *30*, 31–41.
79. Milas, M.; Roure, I.; Berry, G. C. Crossover Behavior in the Viscosity of Semiflexible Polymers: Solutions of Sodium Hyaluronate as a Function of Concentration, Molecular Weight, and Temperature. *J. Rheol.* **1996**, *40*, 1155–1166.
80. Mo, Y.; Takaya, T.; Nishinari, K.; Kubota, K.; Okamoto, A. Effects of Sodium Chloride, Guanidine Hydrochloride, and Sucrose on the Viscoelastic Properties of Sodium Hyaluronate Solutions. *Biopolymers* **1999**, *50*, 23–34.
81. Milas, M.; Rinaudo, M.; Roure, I.; Al-Assaf, S.; Phillips, G. O.; Williams, P. A. Comparative Rheological Behavior of Hyaluronan From Bacterial and Animal Sources With Cross-Linked Hyaluronan (Hylan) in Aqueous Solution. *Biopolymers* **2001**, *59*, 191–204.
82. Krause, W. E.; Bellomo, E. G.; Colby, R. H. Rheology of Sodium Hyaluronate Under Physiological Conditions. *Biomacromolecules* **2001**, *2*, 65–69.
83. Wik, K. O.; Comper, W. D. Hyaluronate Diffusion in Semidilute Solutions. *Biopolymers* **1982**, *21*, 583–599.
84. Gribbon, P.; Heng, B. C.; Hardingham, T. E. The Molecular Basis of the Solution Properties of Hyaluronan Investigated by Confocal Fluorescence Recovery After Photobleaching. *Biophys. J.* **1999**, *77*, 2210–2216.
85. Gribbon, P.; Heng, B. C.; Hardingham, T. E. The Analysis of Intermolecular Interactions in Concentrated Hyaluronan Solutions Suggest No Evidence for Chain–Chain Association. *Biochem. J.* **2000**, *350*(Pt. 1), 329–335.

86. Cowman, M.; Liu, J.; Li, M.; Hittner, D. M.; Kim, J. S. Hyaluronan Interactions: Self, Water, Ions. In *The Chemistry, Biology and Medical Applications of Hyaluronan and Its Derivatives*; Portland Press: London, 1998.
87. de la Motte, C. A.; Hascall, V. C.; Drazba, J.; Bandyopadhyay, S. K.; Strong, S. A. Mononuclear Leukocytes Bind to Specific Hyaluronan Structures on Colon Mucosal Smooth Muscle Cells Treated With Polyinosinic Acid:Polycytidylic Acid: Inter-Alpha-Trypsin Inhibitor Is Crucial to Structure and Function. *Am. J. Pathol.* **2003**, *163*, 121–133.
88. Majors, A. K.; Austin, R. C.; de la Motte, C. A.; Pyeritz, R. E.; Hascall, V. C.; Kessler, S. P.; Sen, G.; Strong, S. A. Endoplasmic Reticulum Stress Induces Hyaluronan Deposition and Leukocyte Adhesion. *J. Biol. Chem.* **2003**, *278*, 47223–47231.
89. Hascall, V. C.; Majors, A. K.; De La Motte, C. A.; Evanko, S. P.; Wang, A.; Drazba, J. A.; Strong, S. A.; Wight, T. N. Intracellular Hyaluronan: A New Frontier for Inflammation?*Biochim. Biophys. Acta* **2004**, *1673*, 3–12.
90. Selbi, W.; de la Motte, C. A.; Hascall, V. C.; Day, A. J.; Bowen, T.; Phillips, A. O. Characterization of Hyaluronan Cable Structure and Function in Renal Proximal Tubular Epithelial Cells. *Kidney Int.* **2006**, *70*, 1287–1295.
91. Albeiroti, S.; Soroosh, A.; de la Motte, C. A. Hyaluronan's Role in Fibrosis: A Pathogenic Factor or a Passive Player?*Biomed. Res. Int.* **2015**, *2015, 790203.*
92. Kohda, D.; Morton, C. J.; Parkar, A. A.; Hatanaka, H.; Inagaki, F. M.; Campbell, I. D.; Day, A. J. Solution Structure of the Link Module: A Hyaluronan-Binding Domain Involved in Extracellular Matrix Stability and Cell Migration. *Cell* **1996**, *86*, 767–775.
93. Lee, T. H.; Wisniewski, H. G.; Vilcek, J. A Novel Secretory Tumor Necrosis Factor-Inducible Protein (TSG-6) Is a Member of the Family of Hyaluronate Binding Proteins, Closely Related to the Adhesion Receptor CD44. *J. Cell Biol.* **1992**, *116*, 545–557.
94. Wisniewski, H. G.; Vilcek, J. TSG-6: An IL-1/TNF-Inducible Protein With Anti-Inflammatory Activity. *Cytokine Growth Factor Rev.* **1997**, *8*, 143–156.
95. Lesley, J.; Gal, I.; Mahoney, D. J.; Cordell, M. R.; Rugg, M. S.; Hyman, R.; Day, A. J.; Mikecz, K. TSG-6 Modulates the Interaction Between Hyaluronan and Cell Surface CD44. *J. Biol. Chem.* **2004**, *279*, 25745–25754.
96. Baranova, N. S.; Nileback, E.; Haller, F. M.; Briggs, D. C.; Svedhem, S.; Day, A. J.; Richter, R. P. The Inflammation-Associated Protein TSG-6 Cross-Links Hyaluronan via Hyaluronan-Induced TSG-6 Oligomers. *J. Biol. Chem.* **2011**, *286*, 25675–25686.
97. Jessen, T. E.; Odum, L. Role of Tumour Necrosis Factor Stimulated Gene 6 (TSG-6) in the Coupling of Inter-Alpha-Trypsin Inhibitor to Hyaluronan in Human Follicular Fluid. *Reproduction* **2003**, *125*, 27–31.
98. Mukhopadhyay, D.; Asari, A.; Rugg, M. S.; Day, A. J.; Fulop, C. Specificity of the Tumor Necrosis Factor-Induced Protein 6-Mediated Heavy Chain Transfer From Inter-Alpha-Trypsin Inhibitor to Hyaluronan: Implications for the Assembly of the Cumulus Extracellular Matrix. *J. Biol. Chem.* **2004**, *279*, 11119–11128.
99. Rugg, M. S.; Willis, A. C.; Mukhopadhyay, D.; Hascall, V. C.; Fries, E.; Fulop, C.; Milner, C. M.; Day, A. J. Characterization of Complexes Formed Between TSG-6 and Inter-Alpha-Inhibitor That Act as Intermediates in the Covalent Transfer of Heavy Chains Onto Hyaluronan. *J. Biol. Chem.* **2005**, *280*, 25674–25686.
100. Sanggaard, K. W.; Karring, H.; Valnickova, Z.; Thogersen, I. B.; Enghild, J. J. The TSG-6 and I Alpha I Interaction Promotes a Transesterification Cleaving the Protein-Glycosaminoglycan-Protein (PGP) Cross-Link. *J. Biol. Chem.* **2005**, *280*, 11936–11942.
101. Sanggaard, K. W.; Sonne-Schmidt, C. S.; Jacobsen, C.; Thogersen, I. B.; Valnickova, Z.; Wisniewski, H. G.; Enghild, J. J. Evidence for a Two-Step Mechanism Involved in the Formation of Covalent HC x TSG-6 Complexes. *Biochemistry* **2006**, *45*, 7661–7668.

102. Yingsung, W.; Zhuo, L.; Morgelin, M.; Yoneda, M.; Kida, D.; Watanabe, H.; Ishiguro, N.; Iwata, H.; Kimata, K. Molecular Heterogeneity of the SHAP–Hyaluronan Complex. Isolation and Characterization of the Complex in Synovial Fluid From Patients With Rheumatoid Arthritis. *J. Biol. Chem.* **2003**, *278*, 32710–32718.
103. Day, A. J.; de la Motte, C. A. Hyaluronan Cross-Linking: A Protective Mechanism in Inflammation? *Trends Immunol.* **2005**, *26*, 637–643.
104. Itano, N.; Sawai, T.; Yoshida, M.; Lenas, P.; Yamada, Y.; Imagawa, M.; Shinomura, T.; Hamaguchi, M.; Yoshida, Y.; Ohnuki, Y.; Miyauchi, S.; Spicer, A. P.; McDonald, J. A.; Kimata, K. Three Isoforms of Mammalian Hyaluronan Synthases Have Distinct Enzymatic Properties. *J. Biol. Chem.* **1999**, *274*, 25085–25092.
105. Spicer, A. P.; Tien, J. Y. Hyaluronan and Morphogenesis. *Birth Defects Res. C Embryo Today* **2004**, *72*, 89–108.
106. Underhill, C. CD44: The Hyaluronan Receptor. *J. Cell Sci.* **1992**, *103*(Pt. 2), 293–298.
107. Knudson, C. B. Hyaluronan Receptor-Directed Assembly of Chondrocyte Pericellular Matrix. *J. Cell Biol.* **1993**, *120*, 825–834.
108. Naor, D.; Sionov, R. V.; Ish-Shalom, D. CD44: Structure, Function and Association With the Malignant Process. *Adv. Cancer Res.* **1997**, *71*, 241–319.
109. Knudson, C. B.; Knudson, W. Hyaluronan and CD44: Modulators of Chondrocyte Metabolism. *Clin. Orthop. Relat. Res.* **2004**, *427S*, S152–S162.
110. Pasonen-Seppanen, S.; Hyttinen, J. M.; Rilla, K.; Jokela, T.; Noble, P. W.; Tammi, M.; Tammi, R. Role of CD44 in the Organization of Keratinocyte Pericellular Hyaluronan. *Histochem. Cell Biol.* **2012**, *137*, 107–120.
111. Banerji, S.; Hide, B. R.; James, J. R.; Noble, M. E.; Jackson, D. G. Distinctive Properties of the Hyaluronan-Binding Domain in the Lymphatic Endothelial Receptor Lyve-1 and Their Implications for Receptor Function. *J. Biol. Chem.* **2010**, *285*, 10724–10735.
112. Bano, F.; Banerji, S.; Howarth, M.; Jackson, D. G.; Richter, R. P. A Single Molecule Assay to Probe Monovalent and Multivalent Bonds Between Hyaluronan and Its Key Leukocyte Receptor CD44 Under Force. *Sci. Rep.* **2016**, *6, 34176*.
113. Yang, C.; Cao, M.; Liu, H.; He, Y.; Xu, J.; Du, Y.; Liu, Y.; Wang, W.; Cui, L.; Hu, J.; Gao, F. The High and Low Molecular Weight Forms of Hyaluronan Have Distinct Effects on CD44 Clustering. *J. Biol. Chem.* **2012**, *287*, 43094–43107.
114. Zhuo, L.; Kanamori, A.; Kannagi, R.; Itano, N.; Wu, J.; Hamaguchi, M.; Ishiguro, N.; Kimata, K. SHAP Potentiates the CD44-Mediated Leukocyte Adhesion to the Hyaluronan Substratum. *J. Biol. Chem.* **2006**, *281*, 20303–20314.
115. Lawrance, W.; Banerji, S.; Day, A. J.; Bhattacharjee, S.; Jackson, D. G. Binding of Hyaluronan to the Native Lymphatic Vessel Endothelial Receptor LYVE-1 Is Critically Dependent on Receptor Clustering and Hyaluronan Organization. *J. Biol. Chem.* **2016**, *291*, 8014–8030.
116. Chanmee, T.; Ontong, P.; Itano, N. Hyaluronan: A Modulator of the Tumor Microenvironment. *Cancer Lett.* **2016**, *375*, 20–30.
117. Kultti, A.; Rilla, K.; Tiihonen, R.; Spicer, A. P.; Tammi, R. H.; Tammi, M. I. Hyaluronan Synthesis Induces Microvillus-Like Cell Surface Protrusions. *J. Biol. Chem.* **2006**, *281*, 15821–15828.
118. Rilla, K.; Tiihonen, R.; Kultti, A.; Tammi, M.; Tammi, R. Pericellular Hyaluronan Coat Visualized in Live Cells With a Fluorescent Probe Is Scaffolded by Plasma Membrane Protrusions. *J. Histochem. Cytochem.* **2008**, *56*(10), 901.
119. Rilla, K.; Pasonen-Seppanen, S.; Deen, A. J.; Koistinen, V. V.; Wojciechowski, S.; Oikari, S.; Karna, R.; Bart, G.; Torronen, K.; Tammi, R. H.; Tammi, M. I. Hyaluronan Production Enhances Shedding of Plasma Membrane-Derived Microvesicles. *Exp. Cell Res.* **2013**, *319*, 2006–2018.

120. Rilla, K.; Siiskonen, H.; Tammi, M.; Tammi, R. Hyaluronan-Coated Extracellular Vesicles—A Novel Link Between Hyaluronan and Cancer. *Adv. Cancer Res.* **2014**, *123*, 121–148.
121. Koistinen, V.; Jokela, T.; Oikari, S.; Karna, R.; Tammi, M.; Rilla, K. Hyaluronan-Positive Plasma Membrane Protrusions Exist on Mesothelial Cells In Vivo. *Histochem. Cell Biol.* **2016**, *145*, 531–544.
122. Siiskonen, H.; Rilla, K.; Karna, R.; Bart, G.; Jing, W.; Haller, M. F.; DeAngelis, P. L.; Tammi, R. H.; Tammi, M. I. Hyaluronan in Cytosol—Microinjection-Based Probing of Its Existence and Suggested Functions. *Glycobiology* **2013**, *23*, 222–231.
123. Siiskonen, H.; Karna, R.; Hyttinen, J. M.; Tammi, R. H.; Tammi, M. I.; Rilla, K. Hyaluronan Synthase 1 (HAS1) Produces a Cytokine-and Glucose-Inducible, CD44-Dependent Cell Surface Coat. *Exp. Cell Res.* **2014**, *320*, 153–163.
124. Hascall, V. C.; Wang, A.; Tammi, M.; Oikari, S.; Tammi, R.; Passi, A.; Vigetti, D.; Hanson, R. W.; Hart, G. W. The Dynamic Metabolism of Hyaluronan Regulates the Cytosolic Concentration of UDP-GlcNAc. *Matrix Biol.* **2014**, *35*, 14–17.
125. Yuan, H.; Amin, R.; Ye, X.; de la Motte, C. A.; Cowman, M. K. Determination of Hyaluronan Molecular Mass Distribution in Human Breast Milk. *Anal. Biochem.* **2015**, *474*, 78–88.
126. Tolg, C.; Hamilton, S. R.; Zalinska, E.; McCulloch, L.; Amin, R.; Akentieva, N.; Winnik, F.; Savani, R.; Bagli, D. J.; Luyt, L. G.; Cowman, M. K.; McCarthy, J. B.; Turley, E. A. A RHAMM Mimetic Peptide Blocks Hyaluronan Signaling and Reduces Inflammation and Fibrogenesis in Excisional Skin Wounds. *Am. J. Pathol.* **2012**, *181*, 1250–1270.
127. Noble, P. W.; McKee, C. M.; Cowman, M.; Shin, H. S. Hyaluronan Fragments Activate an NF-Kappa B/I-Kappa B Alpha Autoregulatory Loop in Murine Macrophages. *J. Exp. Med.* **1996**, *183*, 2373–2378.
128. McKee, C. M.; Penno, M. B.; Cowman, M.; Burdick, M. D.; Strieter, R. M.; Bao, C.; Noble, P. W. Hyaluronan (HA) Fragments Induce Chemokine Gene Expression in Alveolar Macrophages. The Role of HA Size and CD44. *J. Clin. Invest.* **1996**, *98*, 2403–2413.
129. Stern, R.; Asari, A. A.; Sugahara, K. N. Hyaluronan Fragments: An Information-Rich System. *Eur. J. Cell Biol.* **2006**, *85*, 699–715.
130. Toole, B. P. Hyaluronan-CD44 Interactions in Cancer: Paradoxes and Possibilities. *Clin. Cancer Res.* **2009**, *15*, 7462–7468.
131. Taylor, K. R.; Yamasaki, K.; Radek, K. A.; Di Nardo, A.; Goodarzi, H.; Golenbock, D.; Beutler, B.; Gallo, R. L. Recognition of Hyaluronan Released in Sterile Injury Involves a Unique Receptor Complex Dependent on Toll-Like Receptor 4, CD44, and MD-2. *J. Biol. Chem.* **2007**, *282*, 18265–18275.
132. Powell, J. D.; Horton, M. R. Threat Matrix: Low-Molecular-Weight Hyaluronan (HA) as a Danger Signal. *Immunol. Res.* **2005**, *31*, 207–218.
133. Scheibner, K. A.; Lutz, M. A.; Boodoo, S.; Fenton, M. J.; Powell, J. D.; Horton, M. R. Hyaluronan Fragments Act as an Endogenous Danger Signal by Engaging TLR2. *J. Immunol.* **2006**, *177*, 1272–1281.
134. Lyle, D. B.; Breger, J. C.; Baeva, L. F.; Shallcross, J. C.; Durfor, C. N.; Wang, N. S.; Langone, J. J. Low Molecular Weight Hyaluronic Acid Effects on Murine Macrophage Nitric Oxide Production. *J. Biomed. Mater. Res. A* **2010**, *94*, 893–904.
135. Seino, S.; Takeshita, F.; Asari, A.; Masuda, Y.; Kunou, M.; Ochiya, T. No Influence of Exogenous Hyaluronan on the Behavior of Human Cancer Cells or Endothelial Cell Capillary Formation. *J. Food Sci.* **2014**, *79*, T1469–75.
136. Huang, Z.; Zhao, C.; Chen, Y.; Cowell, J. A.; Wei, G.; Kultti, A.; Huang, L.; Thompson, C. B.; Rosengren, S.; Frost, G. I.; Shepard, H. M. Recombinant Human

Hyaluronidase PH20 Does Not Stimulate an Acute Inflammatory Response and Inhibits Lipopolysaccharide-Induced Neutrophil Recruitment in the Air Pouch Model of Inflammation. *J. Immunol.* **2014**, *192*, 5285–5295.
137. Stern, R.; Jedrzejas, M. J. Hyaluronidases: Their Genomics, Structures, and Mechanisms of Action. *Chem. Rev.* **2006**, *106*, 818–839.
138. Stern, R.; Kogan, G.; Jedrzejas, M. J.; Soltes, L. The Many Ways to Cleave Hyaluronan. *Biotechnol. Adv.* **2007**, *25*, 537–557.
139. Harada, H.; Takahashi, M. CD44-Dependent Intracellular and Extracellular Catabolism of Hyaluronic Acid by Hyaluronidase-1 and -2. *J. Biol. Chem.* **2007**, *282*, 5597–5607.
140. Rai, S. K.; Duh, F. M.; Vigdorovich, V.; Danilkovitch-Miagkova, A.; Lerman, M. I.; Miller, A. D. Candidate Tumor Suppressor HYAL2 Is a Glycosylphosphatidylinositol (GPI)-Anchored Cell-Surface Receptor for Jaagsiekte Sheep Retrovirus, the Envelope Protein of Which Mediates Oncogenic Transformation. *Proc. Natl. Acad. Sci. U. S. A.* **2001**, *98*, 4443.
141. Duterme, C.; Mertens-Strijthagen, J.; Tammi, M.; Flamion, B. Two Novel Functions of Hyaluronidase-2 (Hyal2) Are Formation of the Glycocalyx and Control of CD44-ERM Interactions. *J. Biol. Chem.* **2009**, *284*, 33495–33508.
142. Hida, D.; Danielson, B. T.; Knudson, C. B.; Knudson, W. CD44 Knock-Down in Bovine and Human Chondrocytes Results in Release of Bound HYAL2. *Matrix Biol.* **2015**, *48*, 42–54.
143. Bourguignon, L. Y.; Singleton, P. A.; Diedrich, F.; Stern, R.; Gilad, E. CD44 Interaction With Na^+–H^+ Exchanger (NHE1) Creates Acidic Microenvironments Leading to Hyaluronidase-2 and Cathepsin B Activation and Breast Tumor Cell Invasion. *J. Biol. Chem.* **2004**, *279*, 26991–27007.
144. Yoshida, H.; Nagaoka, A.; Kusaka-Kikushima, A.; Tobiishi, M.; Kawabata, K.; Sayo, T.; Sakai, S.; Sugiyama, Y.; Enomoto, H.; Okada, Y.; Inoue, S. KIAA1199, a Deafness Gene of Unknown Function, Is a New Hyaluronan Binding Protein Involved in Hyaluronan Depolymerization. *Proc. Natl. Acad. Sci. U. S. A.* **2013**, *110*, 5612–5617.
145. Yoshida, H.; Nagaoka, A.; Nakamura, S.; Sugiyama, Y.; Okada, Y.; Inoue, S. Murine Homologue of the Human KIAA1199 Is Implicated in Hyaluronan Binding and Depolymerization. *FEBS Open Bio* **2013**, *3*, 352–356.
146. Nagaoka, A.; Yoshida, H.; Nakamura, S.; Morikawa, T.; Kawabata, K.; Kobayashi, M.; Sakai, S.; Takahashi, Y.; Okada, Y.; Inoue, S. Regulation of Hyaluronan (HA) Metabolism Mediated by HYBID (Hyaluronan-Binding Protein Involved in HA Depolymerization, KIAA1199) and HA Synthases in Growth Factor-Stimulated Fibroblasts. *J. Biol. Chem.* **2015**, *290*, 30910–30923.
147. Yamamoto, H.; Tobisawa, Y.; Inubushi, T.; Irie, F.; Ohyama, C.; Yamaguchi, Y. A Mammalian Homolog of the Zebrafish Transmembrane Protein 2 (TMEM2) Is the Long-Sought-After Cell-Surface Hyaluronidase. *J. Biol. Chem.* **2017**, *292*, 7304–7313.
148. Cherr, G. N.; Meyers, S. A.; Yudin, A. I.; VandeVoort, C. A.; Myles, D. G.; Primakoff, P.; Overstreet, J. W. The PH-20 Protein in Cynomolgus Macaque Spermatozoa: Identification of Two Different Forms Exhibiting Hyaluronidase Activity. *Dev. Biol.* **1996**, *175*, 142–153.
149. Seaton, G. J.; Hall, L.; Jones, R. Rat Sperm 2B1 Glycoprotein (PH20) Contains a C-Terminal Sequence Motif for Attachment of a Glycosyl Phosphatidylinositol Anchor. Effects of Endoproteolytic Cleavage on Hyaluronidase Activity. *Biol. Reprod.* **2000**, *62*, 1667–1676.
150. Cherr, G. N.; Yudin, A. I.; Overstreet, J. W. The Dual Functions of GPI-Anchored PH-20: Hyaluronidase and Intracellular Signaling. *Matrix Biol.* **2001**, *20*, 515–525.

151. Bookbinder, L. H.; Hofer, A.; Haller, M. F.; Zepeda, M. L.; Keller, G. A.; Lim, J. E.; Edgington, T. S.; Shepard, H. M.; Patton, J. S.; Frost, G. I. A Recombinant Human Enzyme for Enhanced Interstitial Transport of Therapeutics. *J. Control. Release* **2006**, *114*, 230–241.
152. Thompson, C. B.; Shepard, H. M.; O'Connor, P. M.; Kadhim, S.; Jiang, P.; Osgood, R. J.; Bookbinder, L. H.; Li, X.; Sugarman, B. J.; Connor, R. J.; Nadjsombati, S.; Frost, G. I. Enzymatic Depletion of Tumor Hyaluronan Induces Antitumor Responses in Preclinical Animal Models. *Mol. Cancer Ther.* **2010**, *9*, 3052–3064.
153. Raghavan, P.; Lu, Y.; Mirchandani, M.; Stecco, A. Human Recombinant Hyaluronidase Injections for Upper Limb Muscle Stiffness in Individuals With Cerebral Injury: A Case Series. *EBioMedicine* **2016**, *9*, 306–313.
154. Volpi, N.; Schiller, J.; Stern, R.; Soltes, L. Role, Metabolism, Chemical Modifications and Applications of Hyaluronan. *Curr. Med. Chem.* **2009**, *16*, 1718–1745.
155. Hrabarova, E.; Juranek, I.; Soltes, L. Pro-Oxidative Effect of Peroxynitrite Regarding Biological Systems: A Special Focus on High-Molar-Mass Hyaluronan Degradation. *Gen. Physiol. Biophys.* **2011**, *30*, 223–238.
156. Halliwell, B.; Gutteridge, J. M. C. Role of Iron in Oxygen Radical Reactions. *Methods Enzymol.* **1984**, *105*, 47–56.
157. Halliwell, B.; Gutteridge, J. M. C. Oxygen Toxicity, Oxygen Radicals, Transition Metals and Disease. *Biochem. J.* **1984**, *219*, 1–14.
158. Halliwell, B.; Gutteridge, J. M. C. The Importance of Free Radicals and Catalytic Metal Ions in Human Diseases. *Mol. Aspects Med.* **1985**, *8*, 89–193.
159. Halliwell, B.; Gutteridge, J. M. C. Role of Free Radicals and Catalytic Metal Ions in Human Disease: An Overview. *Methods Enzymol.* **1990**, *186*, 1–85.
160. Halliwell, B.; Gutteridge, J. M. C. Biologically Relevant Metal Ion-Dependent Hydroxyl Radical Generation. An Update. *FEBS Lett.* **1992**, *307*, 108–112.
161. Halliwell, B.; Gutteridge, J. M. Oxygen Free Radicals and Iron in Relation to Biology and Medicine: Some Problems and Concepts. *Arch. Biochem. Biophys.* **1986**, *246*, 501–514.
162. Gutteridge, J. M. Superoxide-Dependent Formation of Hydroxyl Radicals From Ferric-Complexes and Hydrogen Peroxide: An Evaluation of Fourteen Iron Chelators. *Free Radic. Res. Commun.* **1990**, *9*, 119–125.
163. Armstrong, S. E.; Bell, D. R. Measurement of High-Molecular-Weight Hyaluronan in Solid Tissue Using Agarose Gel Electrophoresis. *Anal. Biochem.* **2002**, *308*, 255–264.
164. Puppo, A.; Halliwell, B. Formation of Hydroxyl Radicals From Hydrogen Peroxide in the Presence of Iron. Is Haemoglobin a Biological Fenton Reagent?*Biochem. J.* **1988**, *249*, 185–190.
165. Moseley, R.; Waddington, R. J.; Embery, G. Degradation of Glycosaminoglycans by Reactive Oxygen Species Derived From Stimulated Polymorphonuclear Leukocytes. *Biochim. Biophys. Acta* **1997**, *1362*, 221–231.
166. Saari, H. Oxygen Derived Free Radicals and Synovial Fluid Hyaluronate. *Ann. Rheum. Dis.* **1991**, *50*, 389–392.
167. Schmut, O.; Hofmann, H. Studies on the Generation of Hydrogen Peroxide During Some Non-enzymic Reactions Changing the Hyaluronic Acid Molecule. *Biochim. Biophys. Acta* **1975**, *411*, 231–235.
168. Swann, D. A. The Degradation of Hyaluronic Acid by Ascorbic Acid. *Biochem. J.* **1967**, *102*, 42C–44C.
169. Niedermeier, W.; Dobson, C.; Laney, R. P. Studies on the Ascorbic Acid-Induced Depolymerization of Hyaluronic Acid. *Biochim. Biophys. Acta* **1967**, *141*, 366–373.

170. Cleland, R. L.; Stoolmiller, A. C.; Roden, L.; Laurent, T. C. Partial Characterization of Reaction Products Formed by the Degradation of Hyaluronic Acid With Ascorbic Acid. *Biochim. Biophys. Acta* **1969**, *192*, 385–394.
171. Harris, M. J.; Herp, A.; Pigman, W. Metal Catalysis in the Depolymerization of Hyaluronic Acid by Autoxidants. *J. Am. Chem. Soc.* **1972**, *94*, 7570–7572.
172. Wong, S. F.; Halliwell, B.; Richmond, R.; Skowroneck, W. R. The Role of Superoxide and Hydroxyl Radicals in the Degradation of Hyaluronic Acid Induced by Metal Ions and by Ascorbic Acid. *J. Inorg. Biochem.* **1981**, *14*, 127–134.
173. Fox, R. B.; Fox, W. K. Dimethyl Sulfoxide Prevents Hydroxyl Radical-Mediated Depolymerization of Hyaluronic Acid. *Ann. N. Y. Acad. Sci.* **1983**, *411*, 14–18.
174. Bartold, P. M.; Wiebkin, O. W.; Thonard, J. C. The Effect of Oxygen-Derived Free Radicals on Gingival Proteoglycans and Hyaluronic Acid. *J. Periodontal Res.* **1984**, *19*, 390–400.
175. Carlin, G.; Djursater, R. Xanthine Oxidase Induced Depolymerization of Hyaluronic Acid in the Presence of Ferritin. *FEBS Lett.* **1984**, *177*, 27–30.
176. Liu, K. M.; Swann, D.; Lee, P.; Lam, K. W. Inhibition of Oxidative Degradation of Hyaluronic Acid by Uric Acid. *Curr. Eye Res.* **1984**, *3*, 1049–1053.
177. Myint, P.; Deeble, D. J.; Beaumont, P. C.; Blake, S. M.; Phillips, G. O. The Reactivity of Various Free Radicals With Hyaluronic Acid: Steady-State and Pulse Radiolysis Studies. *Biochim. Biophys. Acta* **1987**, *925*, 194–202.
178. Uchiyama, H.; Dobashi, Y.; Ohkouchi, K.; Nagasawa, K. Chemical Change Involved in the Oxidative Reductive Depolymerization of Hyaluronic Acid. *J. Biol. Chem.* **1990**, *265*, 7753–7759.
179. Chattopadhyay, D.; Akiba, J.; Ueno, N.; Chakrabarti, B. Metal Ion Catalyzed Liquefaction of Vitreous by Ascorbic Acid: Role of Radicals and Radical Ions. *Ophthalmic Res.* **1992**, *24*, 1–7.
180. Kvam, C.; Granese, D.; Flaibani, A.; Pollesello, P.; Paoletti, S. Hyaluronan Can Be Protected From Free-Radical Depolymerisation by 2,6-Diisopropylphenol, a Novel Radical Scavenger. *Biochem. Biophys. Res. Commun.* **1993**, *193*, 927–933.
181. Lindvall, S.; Rydell, G. Influence of Various Compounds on the Degradation of Hyaluronic Acid by a Myeloperoxidase System. *Chem. Biol. Interact.* **1994**, *90*, 1–12.
182. Saari, H.; Konttinen, Y. T.; Friman, C.; Sorsa, T. Differential Effects of Reactive Oxygen Species on Native Synovial Fluid and Purified Human Umbilical Cord Hyaluronate. *Inflammation* **1993**, *17*, 403–415.
183. Moseley, R.; Waddington, R.; Evans, P.; Halliwell, B.; Embery, G. The Chemical Modification of Glycosaminoglycan Structure by Oxygen-Derived Species In Vitro. *Biochim. Biophys. Acta* **1995**, *1244*, 245–252.
184. Hawkins, C. L.; Davies, M. J. Direct Detection and Identification of Radicals Generated During the Hydroxyl Radical-Induced Degradation of Hyaluronic Acid and Related Materials. *Free Radic. Biol. Med.* **1996**, *21*, 275–290.
185. Agren, U. M.; Tammi, R. H.; Tammi, M. I. Reactive Oxygen Species Contribute to Epidermal Hyaluronan Catabolism in Human Skin Organ Culture. *Free Radic. Biol. Med.* **1997**, *23*, 996–1001.
186. Praest, B. M.; Greiling, H.; Kock, R. Effects of Oxygen-Derived Free Radicals on the Molecular Weight and the Polydispersity of Hyaluronan Solutions. *Carbohydr. Res.* **1997**, *303*, 153–157.
187. Šoltés, L.; Stankovská, M.; Brezová, V.; Schiller, J.; Arnhold, J.; Kogan, G.; Gemeiner, P. Hyaluronan Degradation by Copper(II) Chloride and Ascorbate: Rotational Viscometric, EPR Spin-Trapping, and MALDI–TOF Mass Spectrometric Investigations. *Carbohydr. Res.* **2006**, *341*, 2826–2834.

188. Šoltés, L.; Brezová, V.; Stankovská, M.; Kogan, G.; Gemeiner, P. Degradation of High-Molecular-Weight Hyaluronan by Hydrogen Peroxide in the Presence of Cupric Ions. *Carbohydr. Res.* **2006**, *341*, 639–644.
189. Soltes, L.; Stankovska, M.; Kogan, G.; Mendichi, R.; Volpi, N.; Sasinkova, V.; Gemeiner, P. Degradation of High-Molar-Mass Hyaluronan by an Oxidative System Comprising Ascorbate, Cu(II), and Hydrogen Peroxide: Inhibitory Action of Antiinflammatory Drugs—Naproxen and Acetylsalicylic Acid. *J. Pharm. Biomed. Anal.* **2007**, *44*, 1056–1063.
190. Soltes, L.; Kogan, G.; Stankovska, M.; Mendichi, R.; Rychly, J.; Schiller, J.; Gemeiner, P. Degradation of High-Molar-Mass Hyaluronan and Characterization of Fragments. *Biomacromolecules* **2007**, *8*, 2697–2705.
191. Al-Assaf, S.; Navaratnam, S.; Parsons, B. J.; Phillips, G. O. Chain Scission of Hyaluronan by Carbonate and Dichloride Radical Anions: Potential Reactive Oxidative Species in Inflammation?*Free Radic. Biol. Med.* **2006**, *40*, 2018–2027.
192. Beckman, J. S.; Beckman, T. W.; Chen, J.; Marshall, P. A.; Freeman, B. A. Apparent Hydroxyl Radical Production by Peroxynitrite: Implications for Endothelial Injury From Nitric Oxide and Superoxide. *Proc. Natl. Acad. Sci. U. S. A.* **1990**, *87*(4), 1620.
193. Ischiropoulos, H.; Zhu, L.; Beckman, J. S. Peroxynitrite Formation From Macrophage-Derived Nitric Oxide. *Arch. Biochem. Biophys.* **1992**, *298*, 446–451.
194. Hogg, N.; Darley-Usmar, V. M.; Wilson, M. T.; Moncada, S. Production of Hydroxyl Radicals From the Simultaneous Generation of Superoxide and Nitric Oxide. *Biochem. J.* **1992**, *281*(Pt. 2), 419–424.
195. Yang, G.; Candy, T. E.; Boaro, M.; Wilkin, H. E.; Jones, P.; Nazhat, N. B.; Saadalla-Nazhat, R. A.; Blake, D. R. Free Radical Yields From the Homolysis of Peroxynitrous Acid. *Free Radic. Biol. Med.* **1992**, *12*, 327–330.
196. Fukuto, J. M. Chemistry of Nitric Oxide: Biologically Relevant Aspects. *Adv. Pharmacol.* **1995**, *34*, 1–15.
197. van der Vliet, A.; O'Neill, C. A.; Halliwell, B.; Cross, C. E.; Kaur, H. Aromatic Hydroxylation and Nitration of Phenylalanine and Tyrosine by Peroxynitrite. Evidence for Hydroxyl Radical Production From Peroxynitrite. *FEBS Lett.* **1994**, *339*, 89–92.
198. van der Vliet, A.; Eiserich, J. P.; O'Neill, C. A.; Halliwell, B.; Cross, C. E. Tyrosine Modification by Reactive Nitrogen Species: A Closer Look. *Arch. Biochem. Biophys.* **1995**, *319*, 341–349.
199. Crow, J. P.; Spruell, C.; Chen, J.; Gunn, C.; Ischiropoulos, H.; Tsai, M.; Smith, C. D.; Radi, R.; Koppenol, W. H.; Beckman, J. S. On the pH-Dependent Yield of Hydroxyl Radical Products From Peroxynitrite. *Free Radic. Biol. Med.* **1994**, *16*, 331–338.
200. Crow, J. P.; Beckman, J. S. Reactions Between Nitric Oxide, Superoxide, and Peroxynitrite: Footprints of Peroxynitrite In Vivo. *Adv. Pharmacol.* **1995**, *34*, 17–43.
201. Beckman, J. S.; Chen, J.; Ischiropoulos, H.; Crow, J. P. Oxidative Chemistry of Peroxynitrite. *Methods Enzymol.* **1994**, *233*, 229–240.
202. Li, M.; Rosenfeld, L.; Vilar, R. E.; Cowman, M. K. Degradation of Hyaluronan by Peroxynitrite. *Arch. Biochem. Biophys.* **1997**, *341*, 245–250.
203. Balogh, G. T.; Illes, J.; Szekely, Z.; Forrai, E.; Gere, A. Effect of Different Metal Ions on the Oxidative Damage and Antioxidant Capacity of Hyaluronic Acid. *Arch. Biochem. Biophys.* **2003**, *410*, 76–82.
204. Corsaro, M. M.; Pietraforte, D.; Di Lorenzo, A. S.; Minetti, M.; Marino, G. Reaction of Peroxynitrite With Hyaluronan and Related Saccharides. *Free Radic. Res.* **2004**, *38*, 343–353.
205. Baker, M. S.; Green, S. P.; Lowther, D. A. Changes in the Viscosity of Hyaluronic Acid After Exposure to a Myeloperoxidase-Derived Oxidant. *Arthritis Rheum.* **1989**, *32*, 461–467.

206. Green, S. P.; Baker, M. S.; Lowther, D. A. Depolymerization of Synovial Fluid Hyaluronic Acid (HA) by the Complete Myeloperoxidase (MPO) System May Involve the Formation of a HA-MPO Ionic Complex. *J. Rheumatol.* **1990**, *17*, 1670–1675.
207. Schiller, J.; Arnhold, J.; Arnold, K. Action of Hypochlorous Acid on Polymeric Components of Cartilage. Use of ^{13}C NMR Spectroscopy. *Z. Naturforsch. C* **1995**, *50*, 721–728.
208. Tokita, Y.; Sakashita, H.; Okamoto, A.; Kubota, K. Kinetic Study of a Radical Scavenging Effect of Hyaluronic Acid. *Polym. Int.* **1995**, *38*, 161–164.
209. Tokita, Y.; Okamoto, A. Hydrolytic Degradation of Hyaluronic Acid. *Polym. Degrad. Stab.* **1995**, *48*, 269–273.
210. Tokita, Y.; Okamoto, A. Degradation of Hyaluronic Acid—Kinetic Study and Thermodynamics. *Eur. Polym. J.* **1996**, *32*, 1011–1014.
211. Tommeraas, K.; Melander, C. Kinetics of Hyaluronan Hydrolysis in Acidic Solution at Various pH Values. *Biomacromolecules* **2008**, *9*, 1535–1540.
212. Mathews, M. B.; Decker, L. Conformation of Hyaluronate in Neutral and Alkaline Solutions. *Biochim. Biophys. Acta* **1977**, *498*, 259–263.
213. Lowry, K. M.; Beavers, E. M. Thermal Stability of Sodium Hyaluronate in Aqueous Solution. *J. Biomed. Mater. Res.* **1994**, *28*, 1239–1244.
214. Caspersen, M. B.; Roubroeks, J. P.; Qun, L.; Shan, H.; Fogh, J.; Ruidong, Z.; Tommeraas, K. Thermal Degradation and Stability of Sodium Hyaluronate in Solid State. *Carbohydr. Polym.* **2014**, *107*, 25–30.
215. Chabreček, P.; Šoltés, L.; Kállay, Z.; Novák, I. Gel Permeation Chromatographic Characterization of Sodium Hyaluronate and Its Fractions Prepared by Ultrasonic Degradation. *Chromatographia* **1990**, *30*, 201–204.
216. Orviský, E.; Šoltés, L.; Chabreček, P.; Novák, I.; Stančíková, M. Size Exclusion Chromatographic Characterization of Sodium Hyaluronate Fractions Prepared by High Energetic Sonication. *Chromatographia* **1993**, *37*, 20–22.
217. Kubo, K.; Nakamura, T.; Takagaki, K.; Yoshida, Y.; Endo, M. Depolymerization of Hyaluronan by Sonication. *Glycoconjugate J.* **1993**, *10*, 435–439.
218. Gura, E.; Hückel, M.; Müller, P. J. Specific Degradation of Hyaluronic Acid and Its Rheological Properties. *Polym. Degrad. Stab.* **1998**, *59*, 297–302.
219. Wedlock, D. J.; Phillips, G. O.; Davies, A.; Gormally, J.; Wyn-Jones, E. Depolymerization of Sodium Hyaluronate During Freeze Drying. *Int. J. Biol. Macromol.* **1983**, *5*, 186–188.
220. Doherty, M. M.; Hughes, P. J.; Kim, S. R.; Mainwaring, D. E.; Charman, W. N. Effect of Lyophilization on the Physical Characteristics of Medium Molecular Mass Hyaluronates. *Int. J. Pharm.* **1994**, *111*, 205–211.
221. Tokita, Y.; Ohshima, K.; Okamoto, A. Degradation of Hyaluronic Acid During Freeze Drying. *Polym. Degrad. Stab.* **1997**, *55*, 159–164.
222. Balazs, E. A.; Laurent, T. C.; Howe, A. F.; Varga, L. Irradiation of Mucopolysaccharides With Ultraviolet Light and Electrons. *Radiat. Res.* **1959**, *11*, 149–164.
223. Khan, K. A.; Parsons, B. J.; Phillips, G. O.; Keith Davies, A. A Comparison of the Ultra-Violet Radiation Stabilities of Hyaluronic Acid and Chondroitin-4-Sulphate in Aqueous Solution. *Polym. Photochem.* **1981**, *1*, 33–41.
224. Schmut, O.; Ansari, A. N.; Faulborn, J. Degradation of Hyaluronate by the Concerted Action of Ozone and Sunlight. *Ophthalmic Res.* **1994**, *26*, 340–343.
225. Von Sonntag, C.; Bothe, E.; Ulanski, P.; Deeble, D. J. Pulse Radiolysis in Model Studies Toward Radiation Processing. *Radiat. Phys. Chem.* **1995**, *46*, 527–532.
226. Balazs, E. A.; Davies, J. V.; Phillips, G. O.; Young, M. D. Transient Intermediates in the Radiolysis of Hyaluronic Acid. *Radiat. Res.* **1967**, *31*, 243–255.
227. Daar, E.; King, L.; Nisbet, A.; Thorpe, R. B.; Bradley, D. A. Viscosity Changes in Hyaluronic Acid: Irradiation and Rheological Studies. *Appl. Radiat. Isot.* **2010**, *68*, 746–750.

228. Marmur, J. A Procedure for the Isolation of Deoxyribonucleic Acid From Microorganisms. *J. Mol. Biol.* **1961**, *3*, 208–218.
229. Marmur, J. A Procedure for the Isolation of Deoxyribonucleic Acid From Microorganisms. *Methods Enzymol.* **1963**, *6*, 726–738.
230. Balazs, E. A. Ultrapure Hyaluronic Acid and the Use Thereof. US Patent 4,141,973, 1979.
231. Laurent, U. B.; Tengblad, A. Determination of Hyaluronate in Biological Samples by a Specific Radioassay Technique. *Anal. Biochem.* **1980**, *109*, 386–394.
232. Takeuchi, J.; Sobue, M.; Sato, E.; Shamoto, M.; Miura, K. Variation in Glycosaminoglycan Components of Breast Tumors. *Cancer Res.* **1976**, *36*, 2133–2139.
233. Holmes, M. W.; Bayliss, M. T.; Muir, H. Hyaluronic Acid in Human Articular Cartilage. Age-Related Changes in Content and Size. *Biochem. J.* **1988**, *250*, 435–441.
234. Li, X. Q.; Thonar, E. J.; Knudson, W. Accumulation of Hyaluronate in Human Lung Carcinoma as Measured by a New Hyaluronate ELISA. *Connect. Tissue Res.* **1989**, *19*, 243–253.
235. Hiltunen, E. L.; Anttila, M.; Kultti, A.; Ropponen, K.; Penttinen, J.; Yliskoski, M.; Kuronen, A. T.; Juhola, M.; Tammi, R.; Tammi, M.; Kosma, V. M. Elevated Hyaluronan Concentration Without Hyaluronidase Activation in Malignant Epithelial Ovarian Tumors. *Cancer Res.* **2002**, *62*, 6410–6413.
236. Tammi, R.; Pasonen-Seppanen, S.; Kolehmainen, E.; Tammi, M. Hyaluronan Synthase Induction and Hyaluronan Accumulation in Mouse Epidermis Following Skin Injury. *J. Invest. Dermatol.* **2005**, *124*, 898–905.
237. Engstrom-Laurent, A.; Laurent, U. B.; Lilja, K.; Laurent, T. C. Concentration of Sodium Hyaluronate in Serum. *Scand. J. Clin. Lab. Invest.* **1985**, *45*, 497–504.
238. Lauer, M. E.; Mukhopadhyay, D.; Fulop, C.; de la Motte, C. A.; Majors, A. K.; Hascall, V. C. Primary Murine Airway Smooth Muscle Cells Exposed to Poly(I,C) or Tunicamycin Synthesize a Leukocyte-Adhesive Hyaluronan Matrix. *J. Biol. Chem.* **2009**, *284*, 5299–5312.
239. Hitchcock, A. M.; Yates, K. E.; Shortkroff, S.; Costello, C. E.; Zaia, J. Optimized Extraction of Glycosaminoglycans From Normal and Osteoarthritic Cartilage for Glycomics Profiling. *Glycobiology* **2007**, *17*, 25–35.
240. Hitchcock, A. M.; Yates, K. E.; Costello, C. E.; Zaia, J. Comparative Glycomics of Connective Tissue Glycosaminoglycans. *Proteomics* **2008**, *8*, 1384–1397.
241. Guimond, S. E.; Puvirajesinghe, T. M.; Skidmore, M. A.; Kalus, I.; Dierks, T.; Yates, E. A.; Turnbull, J. E. Rapid Purification and High Sensitivity Analysis of Heparan Sulfate From Cells and Tissues: Toward Glycomics Profiling. *J. Biol. Chem.* **2009**, *284*, 25714–25722.
242. Skidmore, M. A.; Guimond, S. E.; Dumax-Vorzet, A. F.; Yates, E. A.; Turnbull, J. E. Disaccharide Compositional Analysis of Heparan Sulfate and Heparin Polysaccharides Using UV or High-Sensitivity Fluorescence (BODIPY) Detection. *Nat. Protoc.* **2010**, *5*, 1983–1992.
243. Coppa, G. V.; Gabrielli, O.; Buzzega, D.; Zampini, L.; Galeazzi, T.; Maccari, F.; Bertino, E.; Volpi, N. Composition and Structure Elucidation of Human Milk Glycosaminoglycans. *Glycobiology* **2011**, *21*, 295–303.
244. Gill, V. L.; Aich, U.; Rao, S.; Pohl, C.; Zaia, J. Disaccharide Analysis of Glycosaminoglycans Using Hydrophilic Interaction Chromatography and Mass Spectrometry. *Anal. Chem.* **2013**, *85*, 1138–1145.
245. Liu, Z.; Zhang, F.; Li, L.; Li, G.; He, W.; Linhardt, R. J. Compositional Analysis and Structural Elucidation of Glycosaminoglycans in Chicken Eggs. *Glycoconjugate J.* **2014**, *31*, 593–602.
246. Turiak, L.; Shao, C.; Meng, L.; Khatri, K.; Leymarie, N.; Wang, Q.; Pantazopoulos, H.; Leon, D. R.; Zaia, J. Workflow for Combined Proteomics and Glycomics Profiling From Histological Tissues. *Anal. Chem.* **2014**, *86*, 9670–9678.

247. Osago, H.; Shibata, T.; Hara, N.; Kuwata, S.; Kono, M.; Uchio, Y.; Tsuchiya, M. Quantitative Analysis of Glycosaminoglycans, Chondroitin/Dermatan Sulfate, Hyaluronic Acid, Heparan Sulfate, and Keratan Sulfate by Liquid Chromatography–Electrospray Ionization-Tandem Mass Spectrometry. *Anal. Biochem.* **2014**, *467*, 62–74.
248. Anower, E. K. M. F.; Kimata, K. Human Blood Glycosaminoglycans: Isolation and Analysis. *Methods Mol. Biol.* **2015**, *1229*, 95–103.
249. Calabro, A.; Hascall, V. C.; Midura, R. J. Adaptation of FACE Methodology for Microanalysis of Total Hyaluronan and Chondroitin Sulfate Composition From Cartilage. *Glycobiology* **2000**, *10*, 283–293.
250. Calabro, A.; Benavides, M.; Tammi, M.; Hascall, V. C.; Midura, R. J. Microanalysis of Enzyme Digests of Hyaluronan and Chondroitin/Dermatan Sulfate by Fluorophore-Assisted Carbohydrate Electrophoresis (FACE). *Glycobiology* **2000**, *10*, 273–281.
251. Gao, N.; Lehrman, M. A. Alternative Sources of Reagents and Supplies of Fluorophore-Assisted Carbohydrate Electrophoresis (FACE). *Glycobiology* **2003**, *13*, 1G–3G.
252. Tengblad, A. Quantitative Analysis of Hyaluronate in Nanogram Amounts. *Biochem. J.* **1980**, *185*, 101–105.
253. Delpech, B.; Bertrand, P.; Maingonnat, C. Immunoenzymoassay of the Hyaluronic Acid–Hyaluronectin Interaction: Application to the Detection of Hyaluronic Acid in Serum of Normal Subjects and Cancer Patients. *Anal. Biochem.* **1985**, *149*, 555–565.
254. Goldberg, R. L. Enzyme-Linked Immunosorbent Assay for Hyaluronate Using Cartilage Proteoglycan and an Antibody to Keratan Sulfate. *Anal. Biochem.* **1988**, *174*, 448–458.
255. Kongtawelert, P.; Ghosh, P. A Method for the Quantitation of Hyaluronan (Hyaluronic Acid) in Biological Fluids Using a Labeled Avidin-Biotin Technique. *Anal. Biochem.* **1990**, *185*, 313–318.
256. Fosang, A. J.; Hey, N. J.; Carney, S. L.; Hardingham, T. E. An ELISA Plate-Based Assay for Hyaluronan Using Biotinylated Proteoglycan G1 Domain (HA-Binding Region). *Matrix* **1990**, *10*, 306–313.
257. Chichibu, K.; Matsuura, T.; Shichijo, S.; Yokoyama, M. M. Assay of Serum Hyaluronic Acid in Clinical Application. *Clin. Chim. Acta* **1989**, *181*, 317–323.
258. Rossler, A. An Ultrasensitive, Nonisotopic Immunoassay for Hyaluronan Using the Streptavidin-Biotin System. *Clin. Chim. Acta* **1998**, *270*, 101–114.
259. Kamada, H.; Masuda, K.; D'Souza, A. L.; Lenz, M. E.; Pietryla, D.; Otten, L.; Thonar, E. J. Age-Related Differences in the Accumulation and Size of Hyaluronan in Alginate Culture. *Arch. Biochem. Biophys.* **2002**, *408*, 192–199.
260. Grigoreas, G. H.; Anagnostides, S. T.; Vynios, D. H. A Solid-Phase Assay for the Quantitative Analysis of Hyaluronic Acid at the Nanogram Level. *Anal. Biochem.* **2003**, *320*, 179–184.
261. Lindqvist, U.; Chichibu, K.; Delpech, B.; Goldberg, R. L.; Knudson, W.; Poole, A. R.; Laurent, T. C. Seven Different Assays of Hyaluronan Compared for Clinical Utility. *Clin. Chem.* **1992**, *38*, 127–132.
262. Haserodt, S.; Aytekin, M.; Dweik, R. A. A Comparison of the Sensitivity, Specificity, and Molecular Weight Accuracy of Three Different Commercially Available Hyaluronan ELISA-Like Assays. *Glycobiology* **2011**, *21*, 175–183.
263. Yuan, H.; Tank, M.; Alsofyani, A.; Shah, N.; Talati, N.; Lobello, J. C.; Kim, J. R.; Oonuki, Y.; de la Motte, C. A.; Cowman, M. K. Molecular Mass Dependence of Hyaluronan Detection by Sandwich ELISA-Like Assay and Membrane Blotting Using Biotinylated Hyaluronan Binding Protein. *Glycobiology* **2013**, *23*, 1270–1280.
264. Jadin, L.; Huang, L.; Wei, G.; Zhao, Q.; Gelb, A. B.; Frost, G. I.; Jiang, P.; Shepard, H. M. Characterization of a Novel Recombinant Hyaluronan Binding Protein for Tissue Hyaluronan Detection. *J. Histochem. Cytochem.* **2014**, *62*, 672–683.

265. Baggenstoss, B. A.; Weigel, P. H. Size Exclusion Chromatography-Multiangle Laser Light Scattering Analysis of Hyaluronan Size Distributions Made by Membrane-Bound Hyaluronan Synthase. *Anal. Biochem.* **2006**, *352*, 243–251.
266. Laurent, U. B.; Granath, K. A. The Molecular Weight of Hyaluronate in the Aqueous Humour and Vitreous Body of Rabbit and Cattle Eyes. *Exp. Eye Res.* **1983**, *36*, 481–492.
267. Dahl, L. B.; Dahl, I. M.; Engstrom-Laurent, A.; Granath, K. Concentration and Molecular Weight of Sodium Hyaluronate in Synovial Fluid From Patients With Rheumatoid Arthritis and Other Arthropathies. *Ann. Rheum. Dis.* **1985**, *44*, 817–822.
268. Dahl, L. B.; Dahl, I. M.; Borresen, A. L. The Molecular Weight of Sodium Hyaluronate in Amniotic Fluid. *Biochem. Med. Metab. Biol.* **1986**, *35*, 219–226.
269. Tengblad, A.; Laurent, U. B.; Lilja, K.; Cahill, R. N.; Engstrom-Laurent, A.; Fraser, J. R.; Hansson, H. E.; Laurent, T. C. Concentration and Relative Molecular Mass of Hyaluronate in Lymph and Blood. *Biochem. J.* **1986**, *236*, 521–525.
270. Lee, H. G.; Cowman, M. K. An Agarose Gel Electrophoretic Method for Analysis of Hyaluronan Molecular Weight Distribution. *Anal. Biochem.* **1994**, *219*, 278–287.
271. Bhilocha, S.; Amin, R.; Pandya, M.; Yuan, H.; Tank, M.; LoBello, J.; Shytuhina, A.; Wang, W.; Wisniewski, H. G.; de la Motte, C.; Cowman, M. K. Agarose and Polyacrylamide Gel Electrophoresis Methods for Molecular Mass Analysis of 5- to 500-kDa Hyaluronan. *Anal. Biochem.* **2011**, *417*, 41–49.
272. Kongtawelert, P.; Ghosh, P. An Enzyme-Linked Immunosorbent-Inhibition Assay for Quantitation of Hyaluronan (Hyaluronic Acid) in Biological Fluids. *Anal. Biochem.* **1989**, *178*, 367–372.
273. Crawford, D. H.; Murphy, T. L.; Ramm, L. E.; Fletcher, L. M.; Clouston, A. D.; Anderson, G. J.; Subramaniam, V. N.; Powell, L. W.; Ramm, G. A. Serum Hyaluronic Acid With Serum Ferritin Accurately Predicts Cirrhosis and Reduces the Need for Liver Biopsy in C282Y Hemochromatosis. *Hepatology* **2009**, *49*, 418–425.
274. Sasaki, Y.; Uzuki, M.; Nohmi, K.; Kitagawa, H.; Kamataki, A.; Komagamine, M.; Murakami, K.; Sawai, T. Quantitative Measurement of Serum Hyaluronic Acid Molecular Weight in Rheumatoid Arthritis Patients and the Role of Hyaluronidase. *Int. J. Rheum. Dis.* **2011**, *14*, 313–319.
275. Dahl, I. M.; Laurent, T. C. Concentration of Hyaluronan in the Serum of Untreated Cancer Patients With Special Reference to Patients With Mesothelioma. *Cancer* **1988**, *62*, 326–330.
276. Yahya, R. S.; El-Bindary, A. A.; El-Mezayen, H. A.; Abdelmasseh, H. M.; Eissa, M. A. Biochemical Evaluation of Hyaluronic Acid in Breast Cancer. *Clin. Lab.* **2014**, *60*, 1115–1121.
277. Kumar, S.; West, D. C.; Ponting, J. M.; Gattamaneni, H. R. Sera of Children With Renal Tumours Contain Low-Molecular-Mass Hyaluronic Acid. *Int. J. Cancer* **1989**, *44*, 445–448.
278. Wu, M.; Cao, M.; He, Y.; Liu, Y.; Yang, C.; Du, Y.; Wang, W.; Gao, F. A Novel Role of Low Molecular Weight Hyaluronan in Breast Cancer Metastasis. *FASEB J.* **2015**, *29*, 1290–1298.
279. Lokeshwar, V. B.; Obek, C.; Soloway, M. S.; Block, N. L. Tumor-Associated Hyaluronic Acid: A New Sensitive and Specific Urine Marker for Bladder Cancer. *Cancer Res.* **1997**, *57*, 773–777.
280. Tammi, R.; Agren, U. M.; Tuhkanen, A. L.; Tammi, M. Hyaluronan Metabolism in Skin. *Prog. Histochem. Cytochem.* **1994**, *29*, 1–81.
281. Rauhala, L.; Hamalainen, L.; Salonen, P.; Bart, G.; Tammi, M.; Pasonen-Seppanen, S.; Tammi, R. Low Dose Ultraviolet B Irradiation Increases Hyaluronan Synthesis in Epidermal Keratinocytes via Sequential Induction of Hyaluronan Synthases Has1-3

Mediated by p38 and Ca^{2+}/Calmodulin-Dependent Protein Kinase II (CaMKII) Signaling. *J. Biol. Chem.* **2013**, *288*, 17999–18012.
282. Tammi, R. H.; Kultti, A.; Kosma, V. M.; Pirinen, R.; Auvinen, P.; Tammi, M. I. Hyaluronan in Human Tumors: Pathobiological and Prognostic Messages From Cell-Associated and Stromal Hyaluronan. *Semin. Cancer Biol.* **2008**, *18*, 288–295.
283. Lokeshwar, V. B.; Rubinowicz, D.; Schroeder, G. L.; Forgacs, E.; Minna, J. D.; Block, N. L.; Nadji, M.; Lokeshwar, B. L. Stromal and Epithelial Expression of Tumor Markers Hyaluronic Acid and HYAL1 Hyaluronidase in Prostate Cancer. *J. Biol. Chem.* **2001**, *276*, 11922–11932.
284. Tolg, C.; Yuan, H.; Flynn, S. M.; Basu, K.; Ma, J.; Tse, K. C.; Kowalska, B.; Vulkanesku, D.; Cowman, M. K.; McCarthy, J. B.; Turley, E. A. Hyaluronan Modulates Growth Factor Induced Mammary Gland Branching in a Size Dependent Manner. *Matrix Biol.* **2017**, *63*, 117–132.
285. Balazs, E. A. Viscosupplementation for Treatment of Osteoarthritis: From Initial Discovery to Current Status and Results. *Surg. Technol. Int.* **2004**, *12*, 278–289.
286. Altman, R. D.; Dasa, V.; Takeuchi, J. Review of the Mechanism of Action for Supartz FX in Knee Osteoarthritis. *Cartilage* **2016**, https://doi.org/10.1177/1947603516684588.
287. Asari, A.; Kanemitsu, T.; Kurihara, H. Oral Administration of High Molecular Weight Hyaluronan (900 kDa) Controls Immune System via Toll-Like Receptor 4 in the Intestinal Epithelium. *J. Biol. Chem.* **2010**, *285*, 24751–24758.
288. He, H.; Li, W.; Tseng, D. Y.; Zhang, S.; Chen, S. Y.; Day, A. J.; Tseng, S. C. Biochemical Characterization and Function of Complexes Formed by Hyaluronan and the Heavy Chains of Inter-Alpha-Inhibitor (HC*HA) Purified From Extracts of Human Amniotic Membrane. *J. Biol. Chem.* **2009**, *284*, 20136–20146.
289. Torihashi, S.; Ho, M.; Kawakubo, Y.; Komatsu, K.; Nagai, M.; Hirayama, Y.; Kawabata, Y.; Takenaka-Ninagawa, N.; Wanachewin, O.; Zhuo, L.; Kimata, K. Acute and Temporal Expression of TNF-Alpha-Stimulated Gene 6 Product, TSG-6, in Mesenchymal Stem Cells Creates Microenvironments Required for Their Successful Transplantation Into the Muscle Tissue. *J. Biol. Chem.* **2015**, *290*, 22771–22781.
290. Sunabori, T.; Koike, M.; Asari, A.; Oonuki, Y.; Uchiyama, Y. Suppression of Ischemia-Induced Hippocampal Pyramidal Neuron Death by Hyaluronan Tetrasaccharide Through Inhibition of Toll-Like Receptor 2 Signaling Pathway. *Am. J. Pathol.* **2016**, *186*, 2143–2151.
291. Tolg, C.; Telmer, P.; Turley, E. Specific Sizes of Hyaluronan Oligosaccharides Stimulate Fibroblast Migration and Excisional Wound Repair. *PLoS One* **2014**, *9, e88479.*
292. Laurent, T. C.; Laurent, U. B.; Fraser, J. R. Serum Hyaluronan as a Disease Marker. *Ann. Med.* **1996**, *28*, 241–253.
293. Korner, T.; Kropf, J.; Gressner, A. M. Serum Laminin and Hyaluronan in Liver Cirrhosis: Markers of Progression With High Prognostic Value. *J. Hepatol.* **1996**, *25*, 684–688.
294. Peng, C.; Wallwiener, M.; Rudolph, A.; Cuk, K.; Eilber, U.; Celik, M.; Modugno, C.; Trumpp, A.; Heil, J.; Marme, F.; Madhavan, D.; Nees, J.; Riethdorf, S.; Schott, S.; Sohn, C.; Pantel, K.; Schneeweiss, A.; Chang-Claude, J.; Yang, R.; Burwinkel, B. Plasma Hyaluronic Acid Level as a Prognostic and Monitoring Marker of Metastatic Breast Cancer. *Int. J. Cancer* **2016**, *138*, 2499–2509.
295. Lokeshwar, V. B.; Obek, C.; Pham, H. T.; Wei, D.; Young, M. J.; Duncan, R. C.; Soloway, M. S.; Block, N. L. Urinary Hyaluronic Acid and Hyaluronidase: Markers for Bladder Cancer Detection and Evaluation of Grade. *J. Urol.* **2000**, *163*, 348–356.